

# Mercury, Moon, Mars: Surface expressions of mantle convection and interior evolution of stagnant-lid bodies

Nicola Tosi<sup>1,2</sup> and Sebastiano Padovan<sup>1</sup>

<sup>1</sup>*Deutsches Zentrum für Luft- und Raumfahrt (DLR), Institute of Planetary Research, Berlin, Germany*

<sup>2</sup>*Technische Universität, Department of Astronomy and Astrophysics, Berlin, Germany*

Accepted chapter to appear in

Mantle Convection and Surface Expressions  
H. Marquardt, M. Ballmer, S. Cottar, K. Jasper (eds.)  
*AGU Monograph Series*, 2020.

# Mercury, Moon, Mars: Surface expressions of mantle convection and interior evolution of stagnant-lid bodies

Nicola Tosi<sup>1,2</sup> and Sebastiano Padovan<sup>1</sup>

<sup>1</sup>*Deutsches Zentrum für Luft- und Raumfahrt (DLR), Institute of Planetary Research, Berlin, Germany*

<sup>2</sup>*Technische Universität, Department of Astronomy and Astrophysics, Berlin, Germany*

It is hard to be finite upon an infinite  
subject, and all subjects are infinite

---

*Herman Melville*

## Abstract

The evolution of the interior of stagnant-lid bodies is comparatively easier to model and predict with respect to the Earth's due to the absence of the large uncertainties associated with the physics of plate tectonics, its onset time and efficiency over the planet's history. Yet, the observational record for these bodies is both scarcer and sparser with respect to the Earth's. It is restricted to a limited number of samples and a variety of remote-sensing measurements of billions-of-years-old surfaces whose actual age is difficult to determine precisely. Combining these observations into a coherent picture of the thermal and convective evolution of the planetary interior represents thus a major challenge. In this chapter, we review key processes and (mostly geophysical) observational constraints that can be used to infer the global characteristics of mantle convection and thermal evolution of the interior of Mercury, the Moon and Mars, the three major terrestrial bodies where a stagnant lid has likely been present throughout most of their history.

## 1 Introduction

In contrast to the Earth whose evolution is controlled by plate tectonics and surface recycling, the other rocky bodies of the solar system operate today in a stagnant-lid mode. While Venus has and had a complex and rather poorly understood tectonics, Mercury, the Moon, and Mars are the paradigm of stagnant-lid bodies. They possess a single, continuous lithosphere, not fragmented into tectonic plates, which undergoes deformation to a much lower extent than the Earth's, and below which solid-state mantle convection takes (or took) place (e.g., Breuer and Moore, 2015). With the possible exception of Mars, which could have experienced a brief episode of surface mobilization in its earliest history (Nimmo and Stevenson, 2000; Tosi et al., 2013b; Plesa et al., 2014), the three bodies have been characterized by stagnant-lid convection over the largest part of their evolution as their old and highly cratered surfaces testify.

While Earth's plate tectonics allows for continuous arc, mid-ocean-ridge, and hot-spot volcanism, stagnant-lid bodies experience only the latter form, which causes mantle melting and the production of secondary crust to be largely concentrated during the early evolution and to fade rapidly as the mantle begins to cool and the stagnant lid to thicken. Sinking of cold tectonic plates on Earth causes efficient cooling of the mantle and core. It promotes core convection and associated solidification of an inner core, resulting in the generation of a magnetic field. The presence of a stagnant lid tends to prevent heat loss, maintaining the interior warm with fundamental consequences for the mode and timing of magnetic field generation.

The absence of a recycling mechanism in stagnant-lid bodies makes the surface record of billions of years of evolution shaped by impacts and volcanism available to remote or in-situ inspection (e.g., Fassett, 2016). Measurements by orbiting spacecrafts of gravity, topography, surface composition, and magnetic field, combined with surface imaging and analysis of samples and meteorites (available for the Moon and Mars, but not for Mercury) provide a set of observational constraints that can be combined to investigate the thermal history of the interior and how mantle convection shaped it.

Venus shows a uniformly young surface (e.g., Hauck et al., 1998) as indicated by the random distribution of impact craters (Herrick, 1994). It does not show signs of Earth-like plate tectonics. Sites of potential subduction (e.g., Schubert and Sandwell, 1995), possibly induced by mantle plumes (Davaille et al., 2017), suggest that Venus is neither in a plate-tectonic nor in a classical stagnant-lid regime. The additional lack of a global magnetic field and the extreme paucity of observational constraints on the interior structure (e.g., Venus’ moment of inertia is not known, preventing any meaningful estimate of its core size) strongly limit the possibility to infer the convective evolution of the planet as opposed to pure stagnant-lid bodies such as Mercury, the Moon, and Mars, to which we limit the present work. Besides Venus, we will also omit discussing Jupiter’s moon Io. Although strictly speaking Io is also a stagnant-lid body, its interior dynamics (e.g., Tackley et al., 2001; Moore and Schubert, 2003) and surface tectonics (e.g., Bland and McKinnon, 2016) are largely controlled by tidal dissipation (e.g., Peale et al., 1979; Segatz et al., 1988). The associated heat production is at the origin of Io’s massive volcanic activity, which controls heat loss via the so-called heat piping mechanism (e.g., O’Reilly and Davies, 1981; Moore and Webb, 2013) and sets this body apart from those whose evolution is governed by solid-state convection driven by radiogenic heating and secular cooling.

The chapter is divided in largely self-contained sections according to physical processes and, loosely, on their temporal extent. Accordingly, Section 2 discusses some developments in the understanding of the earliest stages of the evolution characterized by the solidification of magma oceans and its potential consequences for the creation of a primary crust and the onset of mantle convection. Following magma ocean solidification, the mantle will remove heat through convection and associated decompression melting, which contributes to the creation of a secondary crust, a topic discussed in Section 3. Large impacts were common during the first phases of the solar system, sometimes with important implications for the overall evolution of the body. We describe the potential interaction of the impact-delivered energy with mantle convection in Section 4. The evidence for the presence of ancient magnetic fields on all the three bodies and a present magnetic field on Mercury provides insights into the cooling of the core, as discussed in Section 5. Section 6 describes a set of additional, though somewhat more indirect, constraints on the thermal evolution provided by evidences for global contraction and expansion, measurements of the heat flux, and inferences on the lithospheric thickness based on analysis of gravity and topography. We conclude in Section 7 with a summary comparing the evolution of Mercury, the Moon, and Mars in light of the constraints discussed throughout the chapter.

## **2 Magma ocean solidification and onset of solid-state mantle convection**

During the early stages of the solar system, accretionary impacts of planetesimals, high rates of radiogenic heat production, core-mantle differentiation, and giant collisions involving planetary embryos and protoplanets all contribute to store vast amounts of thermal energy into forming bodies. The accompanying temperatures can easily exceed the liquidus of silicates, leading to the formation of magma oceans, which can extend to great depths, possibly over the entire mantle (e.g., Elkins-Tanton, 2012; Solomatov, 2015). The crystallization of a magma ocean sets the stage for the subsequent long-term evolution of the planet: it controls the initial silicate differentiation of the mantle and the generation of the first (primordial) crust (e.g., Wood et al., 1970; Warren, 1985; Elkins-Tanton et al., 2005; Vander Kaaden and McCubbin, 2015), affects the volatile budget of the interior and atmosphere (e.g., Abe and Matsui, 1986; Elkins-Tanton, 2008; Lebrun et al., 2013; Hier-Majumder and Hirschmann, 2017; Nikolaou et al., 2019), and determines the earliest forms of mantle convection and surface tectonics

(Tosi et al., 2013b; Maurice et al., 2017; Ballmer et al., 2017; Boukaré et al., 2018; Morison et al., 2019).

Because of the low viscosity of silicate liquids (e.g., Karki and Stixrude, 2010), turbulent convection initially controls the dynamics of magma oceans, which are expected to be well mixed and adiabatic (e.g., Solomatov, 2015). For relatively small bodies like Mercury, the Moon and Mars, the mantle melting temperature increases with pressure more rapidly than the convective adiabat. Upon cooling, solidification proceeds thus from the base of the magma ocean upwards (Figure 1a). Given the shape of the relevant high-pressure melting curves (Fiquet et al., 2010; Andraut et al., 2011), this scenario likely applies also to the Earth, although the possibility exists for solidification starting at mid-mantle depths (Stixrude et al., 2009), ultimately leading to the formation of a basal magma ocean (see Labrosse et al., 2015, for a review). For simplicity, here we do not distinguish between solidus and liquidus and simply consider the mantle melting temperature as the temperature corresponding to the so-called rheologically critical melt fraction. Above this threshold, which is usually set around 30–40% (e.g., Costa et al., 2009), the crystal-melt mixture exhibits a liquid-like behavior; below it, crystals tend to form a stress-supporting interconnected network with partially molten rocks effectively deforming as a solid (see e.g., Solomatov and Stevenson, 1993).

Depending on whether newly-formed crystals settle or are suspended by the turbulent flow, the magma ocean can undergo fractional or equilibrium (batch) crystallization. In the first case, liquid and crystals effectively separate without equilibrating. The composition of the liquid evolves continuously through the removal of solidified materials, ultimately leading to the silicate differentiation of the solid mantle (Figure 1b). In the second case, crystals and liquid remain in equilibrium resulting in a compositionally-homogeneous mantle. The conditions determining whether settling or entrainment occurs are still poorly understood. The density difference between liquid and solids, the size of crystals, the vigour of convection, the effects of planetary rotation, and the cooling rate of the magma ocean, all of which evolve in complex ways during solidification, may play a role in controlling whether fractional or equilibrium crystallization occurs (e.g., Tonks and Melosh, 1990; Solomatov and Stevenson, 1993; Solomatov et al., 1993; Suckale et al., 2012; Solomatov, 2015; Maas and Hansen, 2015; Cassanelli and Head, 2016; Maas and Hansen, 2019).

The Moon represents the paradigm of terrestrial body that likely experienced a global-scale magma ocean that underwent fractional crystallization (e.g., Warren, 1985). The analysis of Apollo samples and lunar meteorites, as well as remote-sensing measurements revealed that the ancient lunar highlands largely consist of anorthosites composed of plagioclase feldspar, building a 30–40 km thick crust as inferred from the inversion of gravity and topography data from the GRAIL mission (Wieczorek et al., 2013). In a lunar magma ocean that fractionally solidifies from the bottom up, plagioclase begins to crystallize at a pressure of around 1 GPa, when 70–80% of the magma ocean is solid (e.g., Snyder et al., 1992; Elkins-Tanton et al., 2011; Charlier et al., 2018). At these conditions, the residual liquid is denser than plagioclase crystals. These float to the top of the magma ocean forming the bulk of the Moon’s anorthositic crust, which dramatically reduces the heat loss at the surface and retards magma ocean solidification (e.g., Elkins-Tanton et al., 2011) (see also Sections 2.2 and 3.1). Plagioclase flotation is thought to work efficiently only on the Moon or smaller bodies; for larger bodies like Mars, the more rapid increase of pressure with depth causes plagioclase to become stable at shallow depths where the magma ocean has already reached a degree of crystallinity high enough to prevent flotation (Brown and Elkins-Tanton, 2009; Elkins-Tanton, 2012).

Mercury’s surface is unusually dark (e.g., Robinson et al., 2008). Spectral measurements (Murchie et al., 2015; Peplowski et al., 2016) indicate that graphite is the material responsible for this characteristic. Indeed, Vander Kaaden and McCubbin (2015) showed that for Mercury’s melts, graphite is the only mineral that could form a flotation crust in a crystallizing magma ocean. Yet, the composition of Mercury’s surface is largely the product of secondary volcanism (Section 3.2). Widespread lava flows buried over time the primary graphite crust, which seems to have been exposed in some craters. Similar to Mercury, the surface of Mars is also largely volcanic but lacks evidence for primordial materials generated through the fractional crystallization of a magma ocean (Section 3.2).

From the perspective of the convective dynamics and evolution of the solid mantle, the fractional crystallization of a magma ocean can have fundamental consequences beyond the formation of a

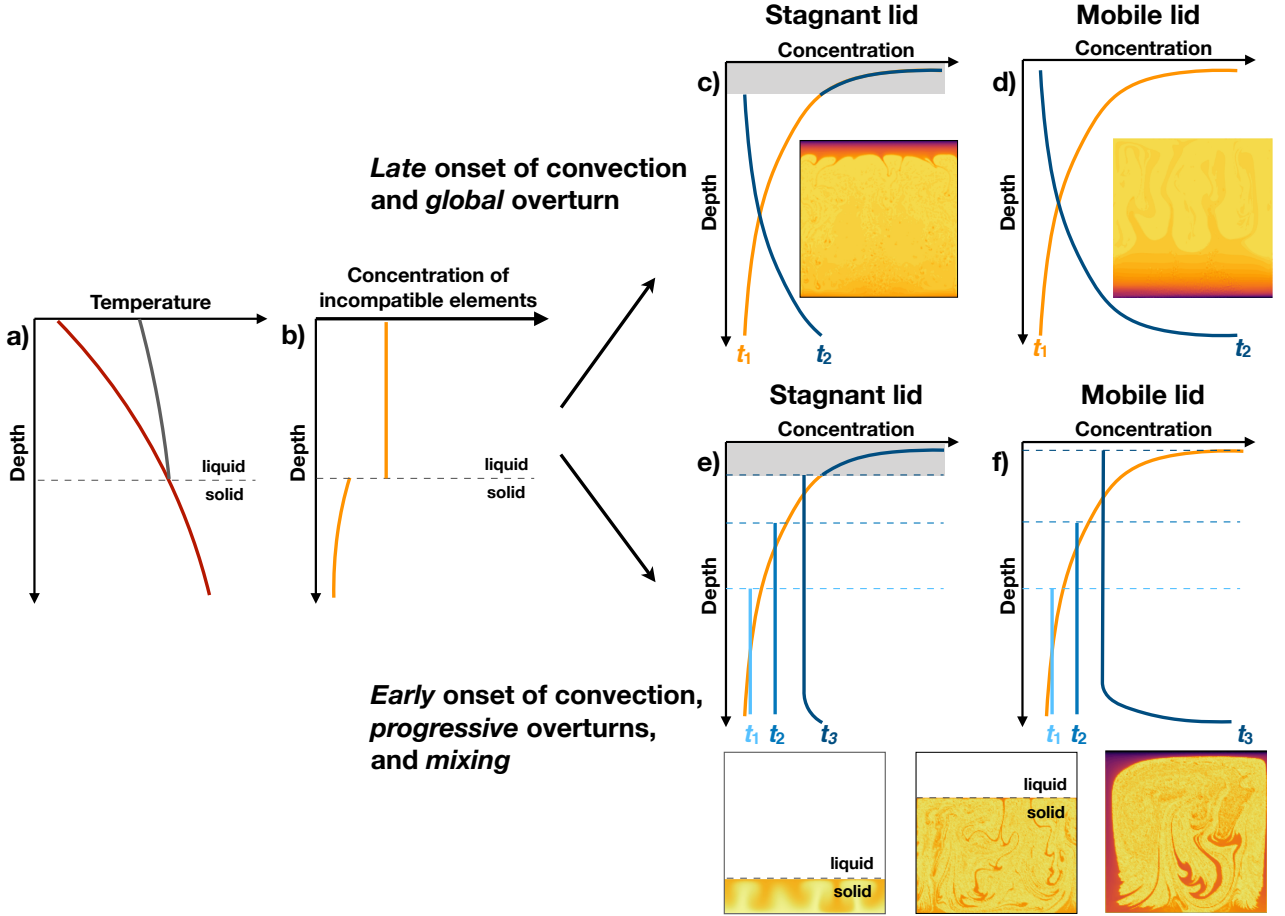


Figure 1: Different scenarios for the consequences of the fractional crystallization of a magma ocean. a) Bottom up solidification due to the steeper slope of the liquid adiabat (grey line) with respect the melting temperature (red line). b) Enrichment of incompatible elements in the liquid phase. c), d) Complete fractional crystallization before the onset of mantle convection. FeO and HPEs are more and more enriched at shallow depths (orange lines at time  $t_1$ ). The formation of a stagnant lid (grey area in panel c) can prevent late-stage cumulates from sinking. The overturn takes place beneath the lid (blue line at time  $t_2$  and contour plot in panel c). If the uppermost cumulates are mobilized, a global-scale overturn takes place (blue line at time  $t_2$  and contour plot in panel d). The contour plots schematically describe the concentration of FeO and HPEs in the solid mantle, with low and high values in light yellow and black, respectively. e), f) As in panels c and d, but for the case of solid-state convection beginning during solidification. Times  $t_1$  to  $t_3$  refer to subsequent stages. An early onset of convection can cause mixing of newly-formed cumulates beneath the magma ocean. The formation of a stagnant lid leaves a largely mixed mantle depleted in incompatible elements (blue line at time  $t_3$  in panel e). Surface mobilization causes the formation of a dense primordial layer, overlaid by a compositionally-homogeneous mantle (blue line at time  $t_3$  in panel f). Snapshots in panels c and d are derived from simulations similar to those of Tosi et al. (2013b); snapshots beneath panels e and f are obtained following the approach of Maurice et al. (2017).

primordial crust. As solids are removed, incompatible elements tend to be progressively enriched in the remaining liquid phase. These include wüstite (FeO) and long-lived heat-producing elements (HPEs) Uranium (U), Thorium (Th) and potassium (K) in addition to volatiles such as water (H<sub>2</sub>O) and carbon dioxide (CO<sub>2</sub>). The concentration  $C_{\text{sol}}$  of incompatible elements at a given radius  $r$  of the solidified cumulates can be expressed as follows (e.g., Boukaré et al., 2018; Morison et al., 2019):

$$C_{\text{sol}}(r) = DC_{\text{liq}}^0 \left( \frac{R_p^3 - R_b^3}{R_p^3 - r^3} \right)^{1-D}, \quad (1)$$

where  $C_{\text{liq}}^0$  is the initial concentration in the liquid magma ocean,  $R_p$  and  $R_b$  are the top and bottom radii of the magma ocean (corresponding to the planet radius and, in the case of a global magma ocean, to the core radius), and  $D$  is a partition coefficient, typically  $\ll 1$ . The concentration of incompatible

elements in solidified cumulates tends thus to follow a power law profile (Figure 1b).

## 2.1 Late onset of mantle convection and global overturn

If fractional crystallization proceeds fast compared to the timescale for the onset of solid-state convection (see below), the progressive enrichment of FeO in the residual liquid ultimately causes the formation of dense, FeO-rich layers at shallow depths overlying deep, FeO-poor layers (Elkins-Tanton et al., 2003, 2005; Tosi et al., 2013b; Plesa et al., 2014; Scheinberg et al., 2014). This configuration is gravitationally unstable and prone to overturn (Figures 1c and 1d). The scenario of fractional crystallization followed by a global-scale overturn has been proposed for Mercury (Brown and Elkins-Tanton, 2009), Mars (Elkins-Tanton et al., 2003, 2005; Elkins-Tanton et al., 2005), the Earth (Elkins-Tanton, 2008; Foley et al., 2014), and the Moon, although in the latter case, the overturn only involves a dense layer forming beneath the plagioclase crust (Zhong et al., 2000; Zhang et al., 2017; Li et al., 2019; Yu et al., 2019; Zhao et al., 2019) (see also Section 3).

Flotation crusts or solid cumulates that crystallize at shallow depth and relatively low temperature have a high viscosity that prevents deformation. Late-stage cumulates enriched in FeO and HPes tend to remain locked in the stagnant lid with the overturn involving only the sub-lithospheric mantle (Figure 1c). A stagnant lid with primordial composition thus forms that overlies a mantle with a moderately stable compositional stratification. Alternatively, the viscosity of the near-surface mantle may remain relatively low due the presence of interstitial melt or to a high surface temperature, allowing for sluggish mobilization (e.g., Scheinberg et al., 2014). Alternatively, the stresses induced by the first upwellings impinging at the base of the lithosphere may locally exceed its yield strength, inducing an early episode of plate-tectonics-like surface mobilization (Tosi et al., 2013b). In both cases a whole-mantle overturn takes place, resulting in a highly stable compositional gradient due to increasing FeO-enrichment of the overturned materials from the surface to the base of the mantle (Figure 1c).

The global-scale overturn of a fractionally crystallized magma ocean—beneath the stagnant lid or involving the lid itself—has been studied in particular in the framework of the early evolution of Mars as it provides a suitable explanation for the generation of an early magnetic field (Elkins-Tanton et al., 2005; Plesa et al., 2014; Scheinberg et al., 2014) (see Section 5), for the rapid formation of secondary crust caused by upwelling cumulates undergoing partial melting upon overturning (Elkins-Tanton et al., 2005) (see Section 3), and for the generation of compositionally-distinct domains in the silicate mantle (e.g., Elkins-Tanton et al., 2003; Debaille et al., 2009). The latter constraint is derived from the analysis of Martian meteorites whose isotopic heterogeneity requires the formation of distinct source-reservoirs within the first  $\sim 100$  Myr of the solar system that remained unmixed throughout the planet’s evolution (e.g., Mezger et al., 2013).

Albeit successful, a global-scale overturn of the above kind poses a problem for the long-term evolution of the Martian mantle. As discussed in Section 3, surface evidence indicates that Mars has been volcanically active throughout its history (Hartmann et al., 1999; Werner, 2009). Long-lived volcanism in a stagnant lid body like Mars is only possible in the presence of a convective mantle where hot plumes rising from the core-mantle boundary (CMB) undergo decompression melting (Plesa et al., 2018). Using the crystallization sequence proposed by Elkins-Tanton et al. (2005), Plesa et al. (2014) performed numerical simulations of global-scale overturn in the Martian mantle in the presence of either a stagnant or a mobile lid. They showed that in both cases the compositional gradient following the overturn (Figure 1c and 1d) is stable enough to largely prevent the subsequent onset of thermal convection and partial melting, at odds with the evidence that volcanism lasted over most of Mars’ history, until as recently as few million years ago (Neukum et al., 2004).

The reason for the above behaviour is to be sought in the large buoyancy ratio associated with the overturned mantle. The buoyancy ratio ( $B$ ) is defined as

$$B = \frac{\Delta\rho_C}{\Delta\rho_T} = \frac{\Delta\rho_C}{\rho_0\alpha\Delta T}, \quad (2)$$

where  $\Delta\rho_C$  is the compositional density difference between shallow, FeO-poor cumulates and deep, FeO-rich cumulates that hinders convection, and  $\Delta\rho_T$  is the density difference due to thermal expansion

between cold shallow cumulates and deep hot cumulates that drives convection ( $\rho_0$  is a reference density,  $\alpha$  the coefficient of thermal expansion, and  $\Delta T$  the temperature difference between the surface and the base of the mantle). For a mantle that underwent a bottom-up solidification,  $\Delta\rho_T$  in eq. (2) can be well determined assuming that the initial core temperature corresponds to the melting temperature of the silicate mantle at CMB conditions. Much more uncertain is the value of  $\Delta\rho_C$ , which can range from 0 for the (unlikely) case of a complete equilibrium crystallization up to several hundreds of  $\text{kg/m}^3$  in the case of a purely fractional crystallization. The crystallization sequence obtained by Elkins-Tanton et al. (2005) assuming pure fractionation and used by Plesa et al. (2014) results in a buoyancy ratio of  $\sim 3$ , sufficiently large to suppress thermal buoyancy and solid-state convection in the overturned mantle. As shown by Tosi et al. (2013b), post-overturn thermo-chemical convection begins to be possible (at least in the upper mantle) for values of  $B$  lower than  $\sim 2$ .

In addition, the dense, FeO-rich cumulates that sink to the CMB are also highly enriched in HPEs. In the presence of a high value of  $B$  preventing the deep mantle from convecting, such cumulates will tend to heat up. The accompanying temperatures can then exceed the solidus, leading to the formation of partial melt, or even the liquidus, leading to the formation of a basal magma ocean (Plesa et al., 2014; Scheinberg et al., 2018), whose consequences for Mars are yet to be explored.

## 2.2 Early onset of mantle convection and progressive mixing

Convective mixing acting while the magma ocean is still solidifying provides a viable way to reduce the effective buoyancy ratio of a solid mantle formed via fractional crystallization. The scenarios described above apply whenever the timescale of magma ocean solidification is shorter than the timescale of convective mobilization of newly formed cumulates. The presence of a growing atmosphere on top of a crystallising magma ocean has been widely recognized as capable to exert a fundamental control on the magma ocean lifetime (e.g., Abe and Matsui, 1986; Elkins-Tanton, 2008; Lebrun et al., 2013; Hamano et al., 2013; Nikolaou et al., 2019). Similar to FeO and HPEs, volatiles are enriched in the liquid phase as the magma ocean cools and solidifies, with their concentration that can increase until reaching saturation in the magma. In this context,  $\text{H}_2\text{O}$  and  $\text{CO}_2$  are the two gases that have been studied most extensively. The amount of gas in excess of saturation is generally assumed to form bubbles that efficiently rise to the surface and escape from the magma ocean forming a secondary atmosphere. This slows down the solidification due to the ability of  $\text{H}_2\text{O}$  and  $\text{CO}_2$  to act as greenhouse gases absorbing infrared radiation. The solidification timescale depends on several poorly constrained parameters (Nikolaou et al., 2019). Above all, it is influenced by the initial bulk abundance of volatiles and by the incoming stellar radiation (e.g., Hamano et al., 2013; Lebrun et al., 2013). For the Earth, for example, model calculations show that a volatile-depleted, whole-mantle magma ocean would solidify in only  $\sim 10^3$  years (e.g., Monteux et al., 2016). By contrast, the presence of an outgassed steam atmosphere corresponding to a bulk water inventory of one Earth’s ocean would extend the solidification to more than 1 Myr (e.g., Elkins-Tanton, 2008; Lebrun et al., 2013; Salvador et al., 2017; Nikolaou et al., 2019). Besides the presence of a thick outgassed atmosphere, the formation of a solid flotation crust can slow down magma ocean solidification even more significantly. In the case of the Moon, a growing flotation crust forming a solid conductive lid on top of the crystallizing magma ocean extends its solidification timescale to at least few tens of millions of years (Meyer et al., 2010; Elkins-Tanton et al., 2011; Perera et al., 2018). For Mercury, the idea of a graphite flotation crust is relatively new, the thickness of such crust highly uncertain (Vander Kaaden and McCubbin, 2015), and dynamic models of Mercury’s convection accounting for the effects of magma ocean solidification still absent. Therefore it remains unclear what its effect would be.

At any rate, a slowly solidifying magma ocean opens the possibility for convection to set in during solidification. Newly formed solid cumulates can overturn and start to be mixed by convection while being overlaid by a liquid magma ocean (Figure 1e and 1f). If mixing is efficient, two end-member configurations at the end of solidification are possible, similar to the previous case of a global overturn. The latest, highly enriched cumulates can remain locked in the stagnant lid, while the underlying mantle has been largely homogenized by an early onset of convection (Figure 1e). Alternatively, if the lid can be mobilized, the uppermost cumulates can sink to the CMB forming a basal layer of materials enriched in incompatible elements (Figure 1f).

Whether or not the solid mantle begins overturning before the end of magma ocean crystallization largely depends on a competition between the timescale of solidification ( $\tau_{\text{MO}}$ ) and the timescale of convective destabilization of the mantle ( $\tau_{\text{conv}}$ ) due to the unstable compositional stratification (Maurice et al., 2017; Ballmer et al., 2017; Boukaré et al., 2018). To quantify the relation between the two timescales, Boukaré et al. (2018) introduced a non-dimensional number ( $R_C$ ) defined as

$$R_C = \frac{\tau_{\text{MO}}}{\tau_{\text{conv}}} = \tau_{\text{MO}} \frac{\Delta\rho_C g D}{\eta}, \quad (3)$$

where  $\tau_{\text{MO}}$  is the magma ocean solidification time,  $\eta$  the dynamic viscosity of the solid mantle,  $\Delta\rho_C$  the density difference between FeO-rich and FeO-poor cumulates (as in eq. (2)),  $g$  the gravity acceleration, and  $D$  the thickness of the solidified mantle. The larger  $R_C$  is, the more likely is that convection will start mixing the mantle during its solidification. As shown by Boukaré et al. (2018) in the framework of isoviscous models, the critical value of  $R_C$  that separates the two scenarios of late onset of convection and global overturn (Figures 1c and 1d) as opposed to an early onset characterized by progressive overturns (Figures 1e and 1f) is between  $10^4$  and  $10^5$ . Figure 2 (which reproduces Figure 3b of Boukaré et al. (2018)), shows the boundary separating the two regimes assuming  $R_C = 5 \times 10^4$ ,  $\Delta\rho = 1000 \text{ kg/m}^3$ , and for  $g$  and  $H$  the gravity acceleration and mantle thickness of the corresponding body. As shown by eq. (3), an early onset is facilitated by long solidification times, a thick mantle and a low viscosity.

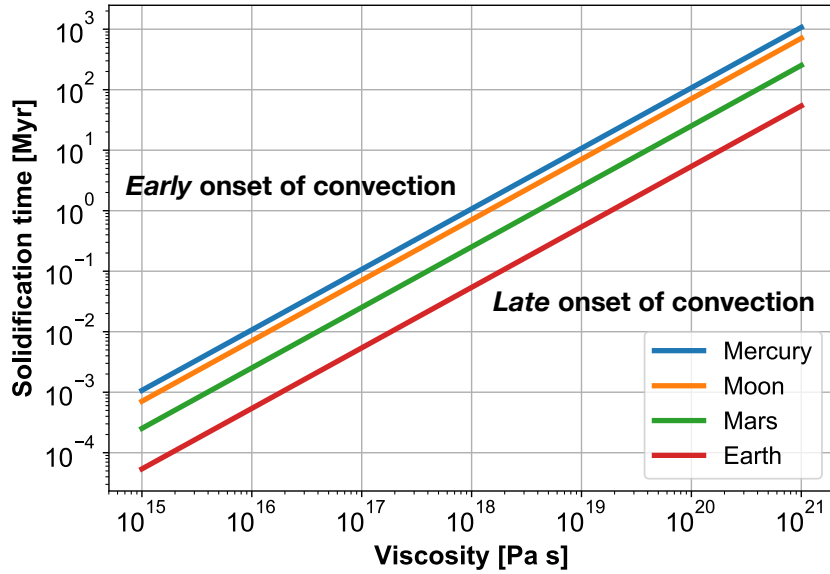


Figure 2: Boundary separating the regime of early onset of convection (above the curve) and late onset of convection (below the curve) for different bodies according to magma ocean solidification time and viscosity of the solid mantle. For a given value of the viscosity, the solidification time allowing for an early onset of convection is longest for Mercury and shortest for the Earth. Similarly, for a given solidification time, the viscosity making an early onset possible is lowest for Mercury and largest for the Earth. The diagram is based on eq. (3) and calculated assuming  $R_C = 5 \times 10^4$ .

The presence of residual melts as well as volatiles renders low values of the viscosity ( $10^{17} \text{ Pa s}$  or even lower) fully plausible (see, e.g., Maurice et al., 2017). For these viscosities, an early onset of convection and mixing (Figures 1e and 1f) becomes likely for Mars (Maurice et al., 2017) in the presence of an outgassed atmosphere retarding magma ocean solidification (e.g., Lebrun et al., 2013)—a scenario that Ballmer et al. (2017) has proposed also for the Earth—and inevitable for the Moon (Boukaré et al., 2018) because of the strong insulating effect of the flotation crust, which remained part of the stagnant lid. Furthermore, recent work that considers the effects of a semi-permeable boundary at the solid-liquid interface via a melting-freezing boundary condition (e.g., Labrosse et al.,



2018; Morison et al., 2019) suggests that the critical Rayleigh number for the onset of solid-state mantle convection can be significantly lower and the heat transfer efficiency significantly higher than for non-penetrative boundaries as assumed in the works of Maurice et al. (2017), Ballmer et al. (2017) and Boukaré et al. (2018). In such a case, an early onset of convection would be facilitated and its effects strengthened. Although a flotation crust was probably present also on Mercury (see also Section 3), the low convective vigor due to the planet’s thin mantle makes the hypothesis of an early onset of convection unlikely and the possibility of a global overturn beneath the stagnant lid and flotation crust (Brown and Elkins-Tanton, 2009) more plausible (Figure 1c). The inferred lack of a highly enriched primary crust on Mars (Section 3) suggests that an early episode of surface mobilization accompanied by the subduction of the latest cumulates (Figure 1f) may have characterized the final stages of magma ocean solidification.

### 3 Crustal manifestations

Being their geologic evolution largely the result of interior processes, planetary crusts contain important clues on the nature and temporal variations of such processes. The focus here is on three aspects of the crust: type, volume, and age of emplacement.

Typically, three types of crust are identified according to a temporal criterion, which also discriminates the different processes associated with their production (e.g., Taylor and McLennan, 2009). As anticipated in Section 2, primary crusts are the result of magma ocean solidification and are emplaced very early in the history of an object; secondary crusts are the result of partial melting of the mantle, which can occur throughout the solar system history; and tertiary crusts are the results of, e.g., remelting of the secondary crust, and at present the only concrete evidence for tertiary crust is the continental crust of the Earth, possibly because plate tectonics is required to produce it (Taylor and McLennan, 2009).

Characterizing the type of crust(s) present in a given body has important implications for models of its thermal evolution, since the crust is chemically different from the bulk composition, most importantly in its content of the long-lived HPEs. Thus, crustal production effectively decreases the value of  $H$ , the specific (i.e., volumetric) rate of internal heat generation appearing in the Rayleigh number for internally heated convection (e.g., Turcotte and Schubert, 2002):

$$\text{Ra}_H = \frac{\rho g \alpha D^5 H}{\eta \kappa \kappa}. \quad (4)$$

In this expression  $\rho$  and  $D$  are the density and thickness of the mantle,  $g$  the gravitational acceleration;  $\alpha$ ,  $\eta$ , and  $\kappa$  are the thermal expansivity, conductivity, and diffusivity;  $\eta$  is the dynamic viscosity. In the case of an early emplaced primary crust, the effect on the internal evolution can be treated as an initial boundary condition on the value of  $H$  (e.g., Laneuville et al., 2013; Rolf et al., 2016). In the case of a secondary crust, which in general is created over an extended period of time, the value of  $H$  has to be time-dependent, consistent with the secondary crust produced (e.g., Morschhauser et al., 2011; Padovan et al., 2017). The absolute amount of heat sources that are extracted in creating crustal material depends critically on the volume of this material and its enrichment with respect to the mantle. These two parameters should be characterized for each crustal type and, at least for the secondary crust, which is emplaced over an extended period of time, for its different units.

The bulk volume of the crust can be investigated using a combination of gravity and topography data. The basic idea is that the non-central components of the gravitational field of a planet contain the contribution of the mass associated with the topography and with any internal non-radially symmetric mass distribution. By ascribing the Bouguer anomaly—the gravitational signal left after the removal of the topographical signal—to subsurface interfaces or loading, models for the thickness of the crust can be obtained. This is usually done either by assuming a given compensation mechanism (e.g., Wiczorek and Phillips, 1997; Padovan et al., 2015), or by globally minimizing the anomalies using an anchor point obtained, e.g., by imposing an average thickness of the crust or by requiring the thickness to be larger than zero everywhere (see, e.g., the review by Wiczorek, 2015). In addition to the bulk volume, it is important to identify the volumes of different units that are associated with different crustal types

and/or different time of emplacement. As a case in point, the lunar maria are dark basaltic provinces located mostly on the near-side of the Moon. They represent the extruded component of magmatic events associated with secondary crustal production, and thus HPEs mantle depletion. In principle, surficial units can be dated through crater counting (Section 4) and their volumes can be estimated by taking advantage of additional stratigraphical, compositional, and geological analyses (e.g., Ernst et al., 2015; Whitten et al., 2011).

The enrichment is typically defined with respect to some model for the bulk abundance of heat-producing elements. The availability of lunar and martian meteorites greatly improves estimates of the bulk abundances of these bodies (e.g., Taylor, 2013; Taylor and Wiczorek, 2014). In the case of Mercury the bulk composition of the silicate part is obtained from a combination of geochemical and geophysical considerations informed by experiments, analysis of the surface composition, and formation and early evolution scenarios (see Nittler et al., 2018, for a recent review). The enrichment of the primary crust depends on a number of physical parameters both extensive—e.g., pressure profile of the body and bulk composition of the magma ocean—and intensive—e.g., density and composition of the last cumulates to solidify. For the secondary crust, which results from the accumulation of melt produced at different times and different locations in the mantle, the enrichment is better defined as a function of local thermodynamic conditions (pressure, temperature, composition, melt fraction), which in turn are a function of the overall evolution of the body.

### 3.1 Primary crusts

Primary crusts are formed as a result of the late-stage solidification of a magma ocean (Section 2). While it is expected that bodies at least as large as Vesta (i.e., with an equivalent diameter larger than about 500 km) go through a magma ocean phase (Elkins-Tanton, 2012), thus possibly producing a primary crust, for bodies larger than Mercury this primary crust is likely overturned and thus, it is not directly observable at present time. The best known, and possibly only certain, example of a primary crust is represented by the lunar anorthositic crust (Wood et al., 1970), which is enriched in HPEs (Taylor and Wiczorek, 2014). In a sense, the lunar primary crust is also an exception, since it represents a flotation crust, created by the upward accumulation of light crystals during the last phases of solidification of the lunar magma ocean. It is generally accepted that also Mercury underwent an initial hot phase characterized by the presence of a global magma ocean (e.g., Brown and Elkins-Tanton, 2009). In the case of Mercury the only mineral that could float and thus originate a lunar-like, gravitationally stable primordial crust is graphite, a very dark mineral (Vander Kaaden and McCubbin, 2015). Overall, the crust of Mercury as observed today is interpreted as being for the most part secondary (e.g., Denevi et al., 2013), with its oldest units having been emplaced in a period consistent with the timing of the late heavy bombardment (LHB) (Marchi et al., 2013). These findings indicate that any primary crust would be difficult to identify. However, the general dark appearance of the Mercurian surface and the existence of extensive dark units, the so called low reflectance material (e.g., Murchie et al., 2015), may represent the sign of a dark, graphitic primary crust subsequently covered by volcanic material and in turn reworked by the intense period of bombardments typical of LHB scenarios (Ernst et al., 2015; Peplowski et al., 2016). The possible volume of the primary crust depends on the unknown bulk carbon content of Mercury. If the carbon content of Mercury lies anywhere between the carbon-poor silicate portion of the Moon and the carbon-rich CI meteorites, then the thickness of the Mercurian primary crust can be anywhere between 1 cm and 10 km (Vander Kaaden and McCubbin, 2015).

The lunar anorthositic crust and the putative graphite primary crust of Mercury are easy to label as primary crusts, since they result from floatating, chemically well-defined minerals. However, the definition of what constitutes a primary crust is both wider and not necessarily unique. What is commonly accepted is that an initial magma ocean phase characterizes all planetary-sized bodies, and the evolving composition of these solidifying magma oceans results in FeO- and HPE-rich late cumulates. Under the simplifying assumption that no convection operates in the solid mantle while the magma ocean is still present (but see Section 2.2), the resulting radial density profile in the solid mantle is gravitationally unstable (e.g., Brown and Elkins-Tanton, 2009; Elkins-Tanton et al., 2011). Apart from the light components, as in the case of the Moon and probably Mercury, this primary

heavy crust is likely to be overturned, i.e., to sink at larger depths until a gravitationally stable profile is reached. Indeed, crystallization models for the lunar magma ocean predict the formation of a dense ilmenite-rich layer (e.g., Elkins-Tanton et al., 2011), which is overlain by the floatation crust (or explicitly, by the “floatating component” of the primary crust). The chemical signature of this layer would make it part of the primary crust. However, its high density and possibly low viscosity would make it sink in the mantle possibly reaching all the way to the core-mantle boundary (e.g., Parmentier et al., 2002; Yu et al., 2019). Depending on its geometry, this overturn could explain the asymmetric nature of the lunar secondary crust (Section 3.2 below).

The rapid accretion of Mars indicates that it sustained a global magma ocean (Dauphas and Pourmand, 2011). Models for the radial density profiles resulting from the solidification of a Martian magma ocean do not predict the formation of a floatation crust and show a strongly gravitationally unstable profile, which would likely rapidly overturn through a Rayleigh-Taylor instability (Elkins-Tanton et al., 2003). As shown in Section 2, since these heavy components of the primary crusts are rich in HPE, their overturn may segregate part of the heat-sources at the bottom of the mantle, as also proposed—but as of yet lacking observational verification—for the Moon, the Earth, and Mars (e.g., Labrosse et al., 2007; Zhang et al., 2013a; Plesa et al., 2014; Yu et al., 2019; Li et al., 2019).

### 3.2 Volume and time of emplacement of the secondary crust

Contrary to the case of the Earth, where plate tectonics operates, melting activity in one-plate bodies is associated only with decompression melting in mantle upwellings (e.g., Baratoux et al., 2013). The melt, if buoyant, contributes to the formation and thickening of the so-called secondary crust through eruptions and/or intrusions. Thus, the volume of the secondary crust as observed today represents the cumulative amount of melt produced in the mantle during the 4.5 Gyr of evolution of the solar system. The thermal state of the mantle largely controls the secondary crustal production (e.g., Laneuville et al., 2013; Grott et al., 2013; Padovan et al., 2017), so putting constraints on the temporal evolution of secondary crustal building would indirectly provide insight on the thermal evolution of the mantle. This approach rests on the possibility of dating the various surface units, typically through crater counting (Section 4), and of interpreting them in terms of interior processes.

The surface of the Earth is continuously reworked by plate tectonics and erosion, and the dating of geological event gets more difficult with older ages, in particular in the Precambrian era, which ended about 600 Ma (e.g., Press and Siever, 1978). Similarly, Venus has a surface younger than about a billion years (e.g., Hauck et al., 1998), which is interpreted as being the result of episodic catastrophic overturns (e.g., Rolf et al., 2018) or continuous volcanic resurfacing (e.g., King, 2018). It is therefore difficult to reconstruct the ancient volcanic history of these two bodies. On the contrary, the geological record of the Moon and Mercury, airless bodies with no plate tectonics, potentially holds the signs of events that occurred during the entire solar system evolution. Mars does not have plate tectonics, unless perhaps for a short time early after its formation (e.g., Nimmo and Stevenson, 2000) (see also Sections 2 and 5), but early in its evolution its surface has been altered by aeolian, fluvial, glacial, and possibly lacustrine—i.e., exogenic—processes (e.g., Craddock and Howard, 2002; Bibring et al., 2006) and the interpretation of its geological record is significantly more complicate than for Mercury and the Moon (e.g., Carr, 2006).

As described above, the crust of the Moon is for the most part primary in nature. The dark patches that can be observed with the naked-eye on the near side of the full Moon represent the surficial manifestations of magmatic events associated with the relatively minor secondary lunar crust production. Overall they accounts for only about 0.7% of the volume of the crust (e.g., Head and Wilson, 1992). Typically, every surficial—or extrusive—volcanic event is associated with a subsurface reservoir of magma, its intrusive counterpart. The amount of intrusive volcanism is difficult if not impossible to assess remotely, and on Earth, where a lot of data are available, the variability of the intrusive-to-extrusive ratio is large (White et al., 2006). Typically a value of 10 times the extruded component can be used as a very rough rule of thumb. Accordingly, the crust of the Moon has a secondary component corresponding to about 7% of its volume. This secondary component, as inferred from crater counting and analysis of samples returned during the Apollo program, shows that the vast majority of the lunar secondary crust has been emplaced in the first 1.5 billions of years of

evolution (e.g., Fig. 18 of Hiesinger et al., 2011).

The secondary crust of the Moon is peculiar in its highly asymmetrical distribution. Almost the entire majority of secondary crustal units are located in the near side, mostly within large impact basins (e.g., Hiesinger et al., 2011). The location of the secondary crust coincides with a region of the surface rich in incompatible elements like Th and U (e.g., Lawrence et al., 1998; Lawrence et al., 2003), which encompasses the Procellarum and Imbrium basins and is commonly referred to as Procellarum KREEP Terrane (PKT), because of its strong enrichment in potassium (K), rare-earth elements (REE) and phosphorous (P) (Jolliff et al., 2000). Additionally, recent magnetic data obtained by the Lunar Prospector and Kaguya missions (Tsunakawa et al., 2015), show a region of weak crustal magnetization roughly corresponding to the PKT (Wieczorek, 2018). The high crustal temperatures associated with a higher abundance of heat producing elements in the PKT region could have prevented retention of a magnetic signature (Wieczorek, 2018). The above set of observations have been interpreted as indicating the presence of material enriched in HPE in the crust or below the crust in the PKT region (Laneuville et al., 2013; Laneuville et al., 2018). In addition to being compatible with the measurements listed above, this scenario can explain a number of additional observations, including asymmetric lunar impact basin morphologies (Miljković et al., 2013) and heat flux variations as directly measured at the Apollo 15 and 17 landing sites and as remotely inferred at one location using the Lunar radiometer experiment onboard the Lunar Reconnaissance Orbiter (Langseth et al., 1976; Warren and Rasmussen, 1987; Paige and Siegler, 2016). While a fully satisfactory explanation for the creation of an enriched layer localized in the near side is currently lacking, several mechanisms have been proposed, both endogenous and exogenous.

Volcanism that is localized on a single lunar hemisphere may be indicative of an early phase of degree-1 convection in the Moon, i.e., convection where buoyant material rises in a single upwelling (Zhong et al., 2000). This scenario may arise if the late dense cumulates resulting from the solidification of the lunar magma ocean and forming beneath the flotation crust would sink to the CMB. For some combination of the rheological properties of the mantle, this material would induced a single mantle upwelling (e.g., Zhang et al., 2013a). In addition, part of these heavy cumulates would remain at the CMB up to the present day (Zhang et al., 2017; Zhao et al., 2019), potentially providing a mechanism to explain the presence of partial melt there, as inferred from the Apollo seismic data (Weber et al., 2011). As initial conditions these models typically assume a post-overtake scenario, where the heavy late cumulates resulting from the solidification of the lunar magma ocean have already sunk to the CMB. However, as described in Section 2.2, the mechanism of the overturn is debated and accordingly, its role in the asymmetrical nature of the lunar evolution is an open question.

Alternatively, the dichotomy has been ascribed to the effect of an impact. Jutzi and Asphaug (2011) investigated the slow-velocity accretion of a companion moon with a mass about 4% of the lunar mass and a diameter of 1270 km, formed in the same protolunar disk and thus, with a composition similar to the Moon. Such a slow-velocity impact on the current far side would explain the thickening of the far-side lunar crust and the displacement of a residual, KREEP-rich magma ocean in the near side. This scenario, while possible, would require the correct timing of the impact with respect to the magma ocean solidification. Some authors have speculated that the compositional and topographical properties of the lunar near side are compatible with an ancient mega-basin (Cadogan, 1974; Whitaker, 1981). Building on this hypothesis, Zhu et al. (2019) explained the observed crustal dichotomy in thickness and composition as the result of an impact of an object with a diameter of about 750 km on the current near-side on an already solidified Moon. The ejecta distribution would explain the crustal thickness dichotomy, and since the excavated KREEP-rich cumulates located below the pre-impact primordial crust would flow back in the resulting giant basin, this model would provide an explanation for the exposure of KREEP-rich material in the near side. However, gravity gradiometry obtained from the GRAIL mission indicates that the subsurface structure in the near side is the result of endogenous magmatic-tectonic structures, likely not compatible with a large impact (Andrews-Hanna et al., 2014). Furthermore, the composition of the far side crust as predicted with the giant impact scenario does not match the observed composition (Zhu et al., 2019).

Similar to the Moon, the secondary crust of Mars has a striking asymmetry. There is a hemispheric difference of about 5 km in surface elevation between the ancient southern highlands and the younger

northern lowlands. This difference is recognized as one of the oldest features of Mars and is reflected in the so-called crustal dichotomy, where, based on gravity and topography data, the crust has an average thickness of about 45 km in the northern lowlands, but is about 25 km thicker under the southern hemisphere (e.g., Neumann et al., 2004; Wieczorek and Zuber, 2004; Plesa et al., 2016). The origin of this difference is the subject of a vast literature. Several mechanisms have been investigated, including exogenous processes involving a giant impact (e.g., Andrews-Hanna et al., 2008a; Marinova et al., 2008) and endogenous ones associated with the formation—as proposed for the Moon—of a hemispherical (i.e., degree-1) upwelling (e.g., Roberts and Zhong, 2006; Keller and Tackley, 2009; Šrámek and Zhong, 2012). Additional hypotheses include a hemispherical overturn of a crystallized magma ocean (e.g., Elkins-Tanton et al., 2003) as proposed for the Moon (e.g., Parmentier et al., 2002), or a combined exogenous-endogenous scenario, with a giant impact triggering a degree-1 convection planform (Golabek et al., 2011; Citron et al., 2018).

Irrespective of the mechanism responsible for the generation of the dichotomy, analysis of Martian meteorites indicates that the crust of Mars is secondary, the bulk of which has been emplaced very early on, likely within 100 Myr of the planet formation (e.g., Nimmo and Tanaka, 2005), and certainly no later than the early Noachian (about 4.2 Ga, Grott et al., 2013). Based on the estimated volume of extruded volcanic units (Greeley and Schneid, 1991), and using a similar intrusive-to-extrusive ratio as for the Moon above, observations can account for about 7% of the volume of the crust, assuming its average thickness is 62 km (Wieczorek and Zuber, 2004; Plesa et al., 2018). While Mars shows signs of very recent volcanic activity (Hartmann et al., 1999; Werner, 2009), possibly extending to the present day (Neukum et al., 2004), the bulk of the secondary crust has been emplaced during the first two billions of years of evolution (Greeley and Schneid, 1991), and mostly very early on as testified by the geological record in the Valles Marineris, which shows that Mars underwent voluminous volcanism during its first billion of years (McEwen et al., 1999).

The analysis of the data returned by the spacecraft MESSENGER, which orbited Mercury between March 2011 and April 2015, indicates that the surface of the innermost planet likely represents the prototype of a secondary crust, since it is interpreted as being largely the result of volcanic events (e.g., Denevi et al., 2013). By dating the different geological units of the surface of the planet, Marchi et al. (2013) showed that the oldest surficial units have been emplaced between 4.0 and 4.1 Ga. This range of ages corresponds roughly with the period of the LHB, and it has been suggested that corresponding to this time any record of older units would have been erased due to the combined effect of impacts and possibly related volcanism (Fassett et al., 2012; Marchi et al., 2013). However, the observational framework supporting the LHB scenario has been recently put into question (Michael et al., 2018; Morbidelli et al., 2018). Independent of the chosen impactor flux, for which several functional shapes have been proposed (e.g., Neukum and Ivanov, 1994; Marchi et al., 2009; Morbidelli et al., 2012), the oldest crust of Mercury is younger than the oldest Lunar crust. Given the secondary nature of the crust, a straightforward explanation is that early on, the hot post-formation mantle produced massive amounts of melt and associated volcanic events that simply kept obliterating older units. However, through melt-induced depletion of heat sources, the mantle cooled (see discussion on the time-dependent  $H$  above) and gradually melt-production decreased. Using similar techniques to those of Marchi et al. (2013), Byrne et al. (2016) inferred that the youngest large volcanic provinces date back to 3.5 Ga. These timings are compatible with recent thermal evolution models of the planet (Tosi et al., 2013a; Padovan et al., 2017).

Figure 3 condenses the present understanding on the composition, origin, and associated volume of the primary and secondary crusts of Mercury, the Moon, and Mars. For Mercury, the secondary crustal volume is based on the central value of Padovan et al. (2015) for the thickness of the crust,  $35 \pm 18$  km. For the thickness of a potential primary crust we use the value of 10 m, based on the possible range between 1 cm and 10 km obtained by Vander Kaaden and McCubbin (2015). The lower end member corresponds to the lower measured lunar carbon content, while the upper end member corresponds to the carbon content of the carbon-rich CI meteorites (Section 3.1). In calculating the volumes, a total silicate thickness of 419 km is assumed, based on the results of Hauck et al. (2013) for the radius of the core and of Perry et al. (2015) for the planetary radius. The thickness of the lunar crust comes from Wieczorek et al. (2013), while the volume of secondary crustal material assumes a

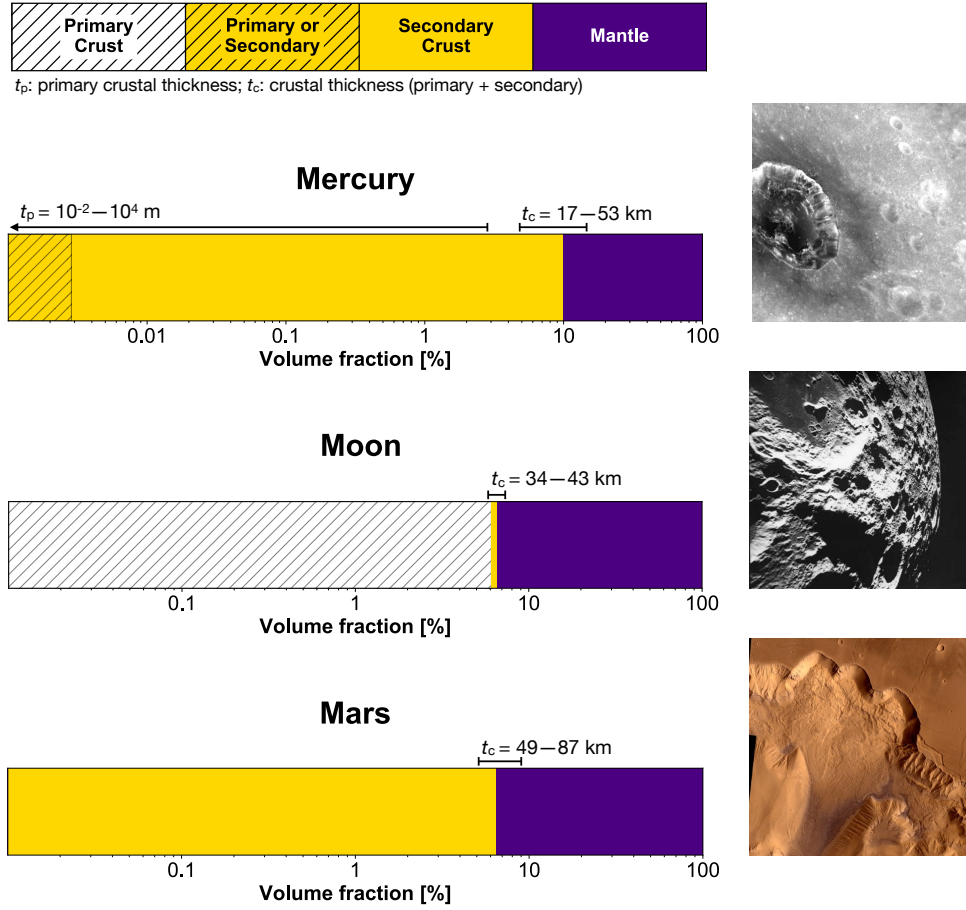


Figure 3: Left column: Volumetric composition of the different silicate reservoirs of Mercury, the Moon, and Mars. Colors indicate composition, according to the legend on top. Note that the scale is logarithmic. The black bars indicate the range of values for the volume fractions, with the labels expressing the corresponding range of thicknesses. Sources for the data are described in the text. Right column: example of the surfaces of each body. Mercury: Berkel crater (diameter  $D = 21$  km), image obtained by the MESSENGER mission. The background represents secondary crust, while the crater is a typical example of exposure of dark material, which has been ascribed to the planet’s primary graphite crust. Moon: the crater on the top left is Aitken ( $D = 135$  km) on the far side of the Moon, in an image obtained by the Apollo 17 mission. The crater is infilled with dark volcanic material, i.e., secondary lunar crust. The light-coloured surrounding area is the primary anorthositic crust. Mars: Ophir Chasma, a valley connected to Valles Marineris, in an image obtained by the Viking 1 mission. This region is associated with massive volcanism early in the history of Mars. The large crater in the lower right corner is 30 km wide. Image credits: Mercury: NASA/Johns Hopkins University APL/Carnegie Institution of Washington Image 5770878 (<https://tinyurl.com/yy96rrkr>); Moon: NASA Image AS17-M-0831, hosted on the LPI website (<https://tinyurl.com/y6mhp7p>); Mars: NASA/JPL/USGS Image PIA00425 (<https://tinyurl.com/yyxnplfw>).

total magmatic reservoir that is ten times the volume of the extruded volcanic material as estimated in Head and Wilson (1992). Values for the volumes are based on a lunar radius of 1737 km (Wieczorek et al., 2006) and a core radius of 330 km (Weber et al., 2011). The Martian crustal thickness range comes from Plesa et al. (2018), and volumes are based on a core radius of 1850 km (Plesa et al., 2018) and a planetary radius of 3390 km (Seidelmann et al., 2007). Interestingly, independent of the particular sources used in creating Figure 3, Mercury, the Moon, and Mars, despite their different sizes, thickness of the mantles, and dominant crustal type, have roughly 7 to 10% of their total silicates contained in the crust.

## 4 Impacts

Craters are created from an impactor population, which has a power-law size distribution comprising relatively few very large objects (e.g., Strom et al., 2015). These large members are responsible for creating some of the largest impact structures observed on the surface of the terrestrial planets, such as the Caloris basin on Mercury (basin diameter  $D_b \sim 1550$  km, Fassett et al., 2012), the South-Pole Aitken basin on the Moon ( $D_b \sim 2200$  km, Garrick-Bethell and Zuber, 2009), and the Hellas basin on Mars ( $D_b \sim 2070$  km, Frey, 2008). Most impacts occur early on, and the cumulative number of impacts occurring on a given surface unit will grow in time, thus potentially providing a way to date the unit based on the statistics of the crater population. Indeed, crater statistics is the most powerful tool to date the surfaces of solid solar system objects (see Fassett, 2016, for a recent review). Comparison of crater statistics for different units of the same object provides relative ages. In the case of the Moon, absolute ages can be obtained through calibration with Apollo samples (e.g., Stöffler and Ryder, 2001). Then, the scaling of the impactor population to different parts of the solar system provides an indirect way to assess the absolute age of surficial units for planets where only crater statistics is available (e.g., Marchi et al., 2009).

Outside of the limited range of impact parameters available in a laboratory setting, the details of impact processes can be simulated using smoothed particle hydrodynamic codes (e.g., Monaghan, 1992), shock-physics codes like iSALE<sup>1</sup> (e.g., Wünnemann et al., 2006), or simple scaling laws (e.g., Pierazzo et al., 1997). Here, we focus on basin-forming impacts, energetic events that have the potential of interacting with the temperature field of the mantle modifying locally its convective vigor (Elkins-Tanton et al., 2004; Ghods and Arkani-Hamed, 2007; Padovan et al., 2017). These are smaller than planetary-scale events like the Moon-forming impact, but larger than the events that create the smaller classes of impact craters observed on the surfaces of airless rocky bodies (e.g. Moon, Mercury, large asteroids). As a rule of thumb, impacts where the size of the impactor is small with respect to the size of the target (i.e., the planet) and that result in the formation of basins (large, multi-ring craters) have the potential of interacting with mantle convection.

The potential effects of impacts on surface magnetization and dynamo action in the core are described in Section 5. Here we discuss the connection between impacts and the thermal state of the mantle, with a focus on the potential surface signatures of this interaction. In so doing, we are explicitly making a qualitative distinction between impacts as a dating tool (Fassett, 2016), which is key in deciphering the history of crustal building (Section 3.2), and (large) impacts as a potential energy source of mantle dynamics.

### 4.1 Basin formation

The formation of an impact basin is a relatively fast process taking place on timescales of few hours, even for the largest basins (e.g., Potter et al., 2012). Schematically, an object hits the surface of a planet at hyper-velocity, creating a so-called transient cavity, which then collapses to form a shallower basin (Melosh, 1989, 2011). In this process, shock waves are produced that travel in the interior, whose energy is released as thermal energy (Bjorkman and Holsapple, 1987) that increases the temperature in a volume roughly centered along the vertical axis of the contact point, possibly causing large scale melting events. The most widely-used code for the accurate simulation of large impacts, events that cannot be reproduced in a laboratory setting, is the iSALE hydrocode (e.g., Wünnemann et al., 2006). Scaling laws aim at condensing in analytical expressions the main effects of impacts as observed in laboratory and numerical experiments. They represent a relatively simple way to describe how the properties of the impactor (size, speed, composition) and of the target (composition, gravity) control a number of physical quantities that are key in the description of the impact process. In this section the goal is to elucidate the connections of large impacts with the interior dynamics, which occurs through the deposition of the impact shock energy in the subsurface. Accordingly, we focus on the properties of the thermal anomaly that forms in the subsurface as a result of the release of the energy of the shock wave.

---

<sup>1</sup>Access to the code can be obtained from <https://isale-code.github.io/access.html>

The computation of the impact-induced thermal anomaly occurs through the following steps. First, a connection is established between the size of the observed basin and the diameter and velocity of the impactor, according to the following scheme, where each arrow indicates a connection through a scaling law: basin diameter  $\rightarrow$  transient cavity diameter  $\rightarrow$  diameter and velocity of the impactor. Estimates for the velocity of the impactor are based on statistical models of the impactors population for the body of interest (Le Feuvre and Wieczorek, 2008; Marchi et al., 2009). The combination of these estimates with the size of the observed basin provides the diameter of the impactor. From the velocity and diameter of the impactor, additional scaling laws provide the distribution of the shock pressure in the subsurface, whose release is responsible for the impact heating, i.e., for the release of energy to the target (e.g., Watters et al., 2009). The following equation highlights the key dependencies in the expression of  $H_{\text{imp}}$ , the energy release associated to a given impact:

$$H_{\text{imp}} = F(\rho_P, \rho_T, g, D_P, v_i), \quad (5)$$

where the gravity  $g$  and density  $\rho_T$  of the target are known. The projectile (i.e., impactor) density  $\rho_P$  is unknown, while its diameter  $D_P$  and impact velocity  $v_i$  are related to the basin diameter as described above. To compute  $H_{\text{imp}}$ , a number of assumptions are usually made. First, despite impacts occurs preferentially at  $45^\circ$  from the vertical (Le Feuvre and Wieczorek, 2008), only the vertical component of the velocity is considered, since it accounts for the majority of the impact-related effects (Shoemaker, 1962, 1983). Secondly, it is often assumed that the impactor has the same composition of the target (i.e., rocky), which can be justified on the basis that objects from the asteroid belt are the main current contributors to the Earth impactors population (e.g., Morbidelli et al., 2002). Both assumptions can be relaxed, and studies exist on the effects of composition and obliquity on the impact processes (e.g., Elbeshausen and Wünnemann, 2011; Ruedas and Breuer, 2018). A recent and clear description of the computation of the energy release for a given impact can be found in, e.g., Roberts and Arkani-Hamed (2017), which accounts for the crater scaling laws (Schmidt and Housen, 1987; Melosh, 1989; Holsapple, 1993), the shock-pressure scaling of Pierazzo et al. (1997), and the foundering shock-heating method of Watters et al. (2009). Care should be taken in using scaling laws appropriate for the problem at hand. For example, the pressure scaling of Pierazzo et al. (1997) should only be used for impactor velocities  $\gtrsim 10$  km/s. The scalings of Monteux et al. (2015), based on iSALE-2D simulations, cover the slow impactor range ( $v_i \gtrsim 4$  km/s).

Given the very different timescales of basin formation processes (few hours) and mantle convection (millions of years), the use of scaling laws represented, until recently, the only viable approach to investigate the interplay of these two processes (e.g., Roberts and Barnouin, 2012; Roberts and Arkani-Hamed, 2017). However, the increase in the computational power available allows one to use outputs of the short timescales simulations (such as those of iSALE) within the long timescales of convection simulations (Rolf et al., 2016; Golabek et al., 2018).

## 4.2 Impact-induced melting

There are three types of melting processes that can be induced by a large impact. First, the release of the impact shock energy increases the temperature of a volume of the target around the impact location, possibly melting it completely (e.g., Roberts and Barnouin, 2012). This process results in what is commonly referred to in the literature as a melt pond or melt sheet (e.g., Cassanelli and Head, 2016). Second, during the formation of a basin a transient crater is excavated, whose maximum depth is larger than the depth of the final basin (e.g., Melosh, 1989). For very large events this transient crater can reach depths of tens of kilometers, thus locally depressing the solidus and potentially inducing massive in-situ decompression melting. This possibility was initially suggested by Ronca (1966)—the seminal work on the connection of impacts and volcanism—and was subsequently discussed several times in relation to the potential connection of impact events with the generation of large igneous provinces (e.g., Rogers, 1982; Rampino, 1987; Elkins-Tanton and Hager, 2005). Third, the positive thermal anomaly resulting from a large impact event locally warps the isotherms producing dynamical currents in the mantle under the newly formed basin, which could lead to additional post-impact convective decompression melting (e.g., Grieve, 1980).



The solidification of the melt sheet could occur through equilibrium crystallization, which preserves the bulk composition of the melt, or through igneous differentiation, which would induce a compositional gradient in the solidified melt sheet (Cassanelli and Head, 2016) (see Section 2). According to the model of Cassanelli and Head (2016), the discrimination between the two possibilities is controlled by the size of the crystals that form in the cooling pond, while the bulk size of the melt sheet plays a minor influence. However, the crystal size is difficult to determine a priori. On the Moon, there are indications for igneous differentiation in the Orientale basin (Spudis et al., 2014) and in the South-Pole Aitken basin (Vaughan and Head, 2014).

The process of in-situ decompression melting is predicated on the assumption that in the short timescales of transient crater formation rocks at depth undergo melting due to the rapid removal of lithostatic pressure. However, Ivanov and Melosh (2003) argue that a more appropriate estimate is based on the profile of the final crater, which, being shallower than the transient crater, would induce significantly less melting. Independent of the feasibility of the in-situ decompression melting process, it is important to note that both the solidification of the melt sheet and the eruption of the in-situ decompressed melt would occur on geologically short timescales (Reese and Solomatonov, 2006; Elkins-Tanton et al., 2004; Elkins-Tanton and Hager, 2005). Thus, dating of units related to the first two processes would coincide with the age of the basin itself.

### 4.3 Impact-related effects on global mantle dynamics

The observations that most basaltic units on the near side of the Moon are located within large impact basins and have been emplaced from several tens to up to hundreds of millions of years after the basins formation, hinted at a possible causal connection between impacts and subsequent volcanism. This process would result from the interaction of the impact-induced thermal anomaly with the mantle temperature field, the process referred to above as post-impact convective decompression melting. While a qualitative assessment of post-impact convective decompression melting has been published early on (Grieve, 1980), more quantitative work has appeared only in the last 20 years.

Reese et al. (2002, 2004) showed that a thermal anomaly induced by a very ancient impact event can explain the long-term volcanism observed in the Tharsis province on Mars (Hartmann et al., 1999; Werner, 2009). However, conventional thermal evolution models do not require a large impact to justify the long-term volcanism on Tharsis, and are also compatible with several additional constraints (e.g., Plesa et al., 2018). More recently, Roberts and Arkani-Hamed (2012, 2017) investigated the role of large impacts on the dynamics of the mantle and energetics of the core of Mars. While large impacts can focus upwellings under the impact locations (Roberts and Arkani-Hamed, 2012), a confirmation of the results of Reese et al. (2004), and can temporarily frustrate dynamo action in the core, the duration of a Martian dynamo is controlled by the rheological properties of the lower mantle (Roberts and Arkani-Hamed, 2017). Similar models for Mercury, where the largest confirmed impact basin is the relatively small Caloris basin, with a diameter of about 1500 km (Fassett et al., 2009), show that the effects on the energetics of the core are minor, while inducing a modification of the convection planform under the basin location (Roberts and Barnouin, 2012). Rolf et al. (2016) investigated the effects of the lunar impact history on the long-term evolution of the body, concluding that the full sequence of large impacts may influence the present-day heat flux and the initial expansion of the Moon, two parameters that could be measured and thus, provide additional constraint for thermal evolution models (Section 6). However, Miljković et al. (2013) proved that the different morphologies of the lunar impact basins between the near-side and the far-side can be explained by the asymmetric distribution of heat producing elements in the interior before the basins formed (Laneuville et al., 2013; Laneuville et al., 2018). Accordingly, it seems plausible, at least for the Moon, that while large impacts may induce effects that are still measurable today (Rolf et al., 2016; Ruedas and Breuer, 2019), it is the initial distribution of heat-producing elements that largely controls the overall evolution.

### 4.4 Local signatures of impact-related effects

The studies described in the previous section all dealt with the potential global consequences of one or more large impacts. However, the creation of an impact basin is by definition a local process,

which ejects or melts pre-existing crust (e.g., Potter et al., 2012), thus modifying the local surficial composition and topography. Often, large basins on the Moon and Mercury are associated with the presence of positive gravity anomalies (or mascons, for mass concentrations) and volcanic infillings, which on the Moon are called maria (Melosh et al., 2013; James et al., 2015).

Elkins-Tanton et al. (2004) investigated the potential causal connection of impact processes with subsequent localized enhanced volcanism. They developed a model for the magmatic effects of large impacts, which takes into account the in-situ decompression melting and the post-impact convective decompression melting (see Section 4.2 for definitions). By adjusting the pre-impact lunar mantle temperature profile, Elkins-Tanton et al. (2004) were able to reproduce the source depth and volume of the maria. However, it was difficult to match the interval observed between the formation of the basin and the later emplacement of the volcanic material. The authors recognize that a potential shortcoming of the model lies in their assumption that the mantle, before an impact, is not convecting. Accordingly, any post-impact convective decompression melting is only due to the limited convection activity induced by the warping of the isotherms—and related horizontal temperature gradient—induced by the impact itself.

Using thermal evolution models that include two-phase flow, Ghods and Arkani-Hamed (2007) investigated convective long-term magmatic activity induced by lunar impact basins using as background temperature field a set of models evolved for 500 Myr, when the largest impacts are assumed to occur. This model is able to reproduce the timing of volcanic activity within Imbrium-sized basins and, for certain combination of parameters, the observed volume of volcanic material. As for the case of Elkins-Tanton et al. (2004), the model predicts a large amount of volcanic activity within the large SPA basin, which is not observed.

Padovan et al. (2017) investigated the magmatic effects of the formation of large impact basins on Mercury using as background temperature and velocity field a reference model selected from a large suite of 2D dynamical models. The reference model was selected based on its compatibility with the observed thickness of the crust (as inferred by geoid-to-topography ratios, Padovan et al., 2015), the duration of volcanic activity (as inferred by crater statistics, Byrne et al., 2016), and the depth of the lithospheric thickness at two different epochs (as inferred by petrologic experiments, Namur et al., 2016). Figure 4 illustrates how the formation of a Caloris-sized basin produces a large thermal anomaly in the mantle, which locally alters the magmatic activity for a geologically long timescale. By tracking the amount of melt produced under a basin, Padovan et al. (2017) were able to reproduce the volume and time of emplacement of the volcanic materials within the Caloris and Rembrandt basins on Mercury. This result critically depends on the thermal state of the mantle at the time of the basin formation, thus indicating how basin-specific datasets (namely, volume and time of emplacement of volcanic material) provide information on the global evolution of the body.

## 5 Mantle cooling and magnetic field generation

Besides the Earth, among the solid planets and satellites of the solar system only Mercury and Ganymede possess today a self-sustained magnetic field. In addition, the surfaces of Mercury, the Moon, and Mars exhibit a remnant magnetization due to the presence of magnetic minerals in their crust and lithosphere. On the one hand, an active magnetic field requires organized, large-scale motion of an electrically conducting fluid, generally thought to be the liquid core. On the other hand, a remnant magnetization, detected via remote sensing or measured by direct sample analysis, indicates that a dynamo was active in the past so that the accompanying magnetic field left its imprint in surface and shallow rocks when these formed. The possibility to generate a magnetic dynamo is tightly related to the way mantle convection operates by cooling the core (Stevenson et al., 1983). Therefore, the existence of an internally-generated magnetic field, at present or in the past, can be used as an indicator of convection and cooling of the mantle and as a constraint for its thermal evolution.

Ferromagnetic minerals present in crustal rocks acquire a so-called thermoremanent magnetization (TRM) if cooled from above their Curie temperature ( $T_C$ ) in the presence of an ambient magnetic field. Melts that erupt on a planetary surface or are intruded at depth typically have temperatures largely in excess of  $T_C$  and, in the presence of a background magnetic field, acquire a strong TRM

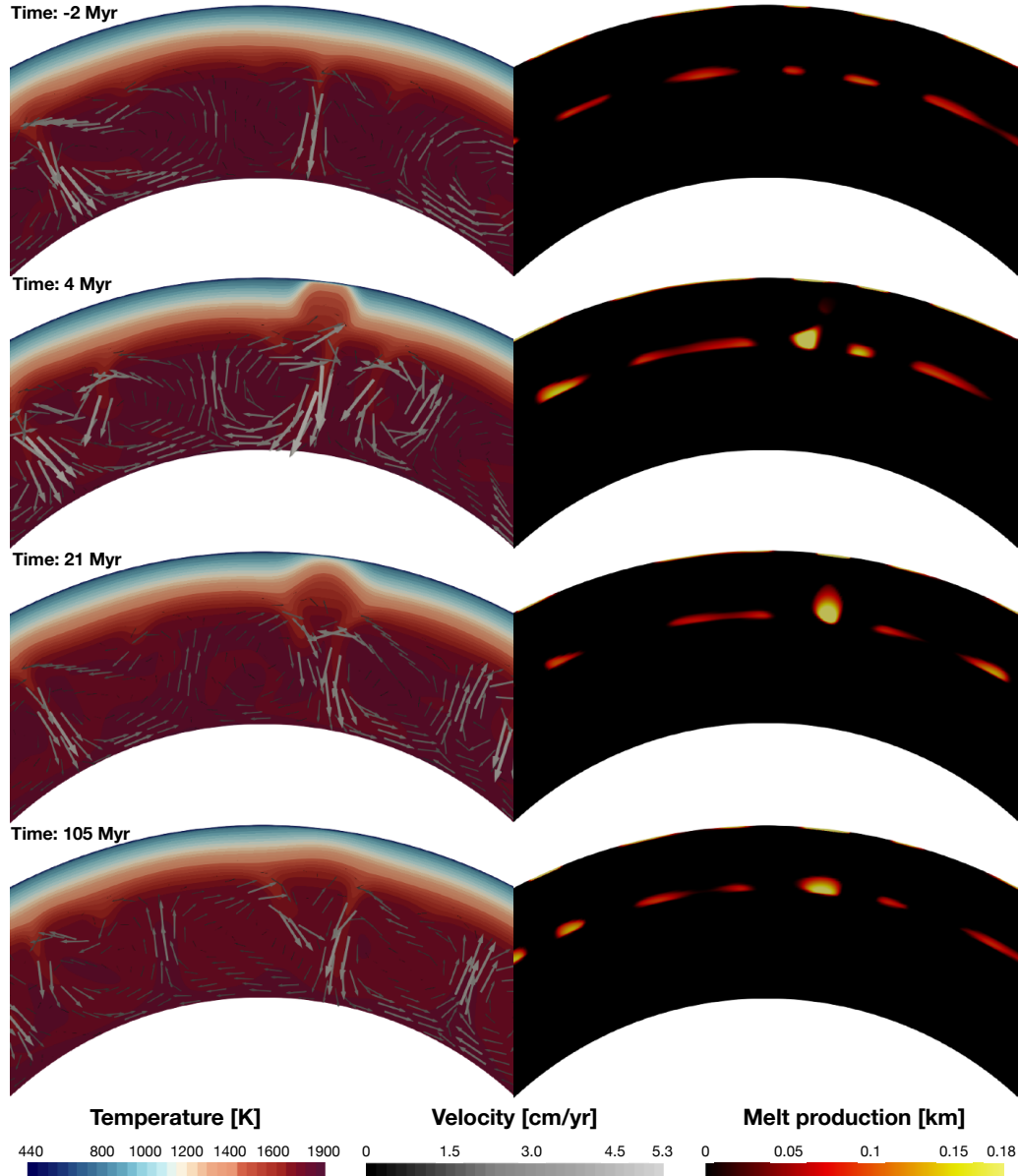


Figure 4: Formation of a Caloris-sized basin on Mercury. Each panel indicates the timing with respect to the basin-forming impact. Left column: Temporal evolution of the temperature field (background) and of the magnitude of the velocity field (arrows). Right column: temporal evolution of the melt production, which is expressed in equivalent crustal thickness. The thermal anomaly warps the isotherms and convective currents, which generate melt, develop in the region close to the impact, but with a certain delay with respect to the impact event. Redrawn after Padovan et al. (2017).

upon cooling below  $T_C$ . If the age of the magnetized rocks is also known—from radiometric techniques or from dating of surface units—it is possible to infer the lifetime of an ancient magnetic field and place constraints on the thermal history of the body.

The generation of a planetary-scale magnetic field is possible in the presence of a large volume of electrically conducting fluid whose motion is driven by an energy source—thermal, compositional, and/or mechanical—and structurally organized through rotation, which provides the positive feedback necessary for the field to be self-sustained (e.g., Olson, 2008). Although promising advances in theory and experiments indicate that core motion and turbulence can be excited by periodic forcing induced by tides, precession, and libration (Le Bars, 2016), buoyancy-driven flows of thermal and/or chemical origin provide today the standard model of core convection and dynamo action (see, e.g. the review by Breuer et al., 2010).

Thermal and compositional convection in a liquid core are driven by mantle cooling. From a

global-scale perspective, thermal convection requires that the average heat flux at the base of the mantle ( $F_{\text{CMB}}$ ) exceeds the heat flux conducted along the adiabat of the convective core ( $F_{\text{ad}}$ ), i.e.,

$$F_{\text{CMB}} = k_{\text{m}} \frac{dT_{\text{CMB}}}{dr} \geq F_{\text{ad}} = k_{\text{c}} \frac{\alpha_{\text{c}} g_{\text{c}} T_{\text{CMB}}}{c_{\text{c}}}, \quad (6)$$

where  $r$  is the radial coordinate,  $k_{\text{m}}$  and  $k_{\text{c}}$  the thermal conductivities of the mantle and core,  $\alpha_{\text{c}}$  the coefficient of thermal expansion of the liquid core,  $g_{\text{c}}$  the gravity acceleration at the CMB,  $T_{\text{CMB}}$  the temperature at the CMB, and  $c_{\text{c}}$  the core specific heat capacity. A large temperature gradient at the base of the mantle helps satisfying this condition. On Earth, the subduction of tectonic plates favours cooling of the interior; it leads to a large temperature difference between the mantle and core and in turn to a high heat flux at the base of the mantle, which facilitates core convection and cooling over Earth’s history (e.g., Nakagawa and Tackley, 2015). In contrast, on stagnant lid bodies, the interior is cooled less efficiently; the mantle tends to remain hotter and the temperature gradient at the CMB smaller, with the consequence that driving thermal convection in the core is generally possible only during the early stages of evolution if the process of core formation left the core largely superheated with respect to the mantle (e.g., Breuer and Spohn, 2003; Williams and Nimmo, 2004) and/or upon the first mantle overturn corresponding to onset of thermal (and possibly compositional) mantle convection (Elkins-Tanton et al., 2005; Plesa et al., 2014). In addition, the presence of heat-producing elements such as K, as well as the release of latent heat upon core freezing (see below) can also contribute to drive thermal convection in the core.

For compositional convection to occur, the core must be 1) composed of a mixture of Fe and one or more light alloying elements—S being the best-studied candidate—and 2) cooled sufficiently to start local freezing. The presence of light elements reduces the density of the core alloy and its melting temperature with respect to those of a core with a pure Fe composition.

Let us consider a standard model of freezing of a Fe-S core. If the pressure slope of the core melting temperature is larger than that of the core adiabat as in the case of the Earth, upon cooling of a fully liquid core, the temperature drops below the liquidus first at the center of the planet, causing the core to freeze from the bottom up in a similar way as a magma ocean would freeze (Figure 1a). As cooling and crystallization continue, the liquid outer core becomes more and more depleted in Fe and enriched in S. Atop of the solidified core, a sulphur-rich layer forms. Being lighter than the overlying fluid, this layer buoyantly rises driving compositional convection that tends to homogenize the remaining fluid and can potentially power a dynamo.

In the framework of the Fe-S system, a different crystallization scenario is also possible. Melting experiments indicate that at pressures smaller than  $\sim 14$  GPa—relevant for the cores of Mercury, the Moon, and Mars—the pressure slope of the core melting temperature is negative (Chen et al., 2008; Buono and Walker, 2011). As a consequence, the adiabatic temperature of a cooling core would first drop below the liquidus at the CMB rather than at the center. Fe crystals would then form at the CMB and precipitate, generating an “iron-snow” (see e.g. Breuer et al., 2015, for a review). Since the melting temperature of an Fe-S liquid is lower than that of pure Fe, newly formed Fe crystals would rapidly remelt, enriching the remaining fluid in Fe. Dense, Fe-rich fluid atop lighter Fe-FeS fluid creates a gravitationally unstable configuration that triggers compositional convection and possibly dynamo action (e.g., Rückriemen et al., 2018).

## 5.1 Mercury’s present-day and early magnetic field

The current knowledge of Mercury’s magnetic field is largely the result of more than four years spent by the MESSENGER spacecraft orbiting the planet (see Johnson et al., 2018, for a recent review). The field is weak, axisymmetric, dipolar, and characterized by a large quadrupolar component corresponding to a northward offset of the magnetic equator with respect to the geographic equator of about 20% of the planetary radius (Anderson et al., 2012). Taken together, these features pose a significant challenge for numerical dynamo models (Wicht and Heyner, 2014). On the one hand, standard models of core flow driven by compositional convection associated with an Earth-like growth of the inner core can produce under certain conditions a weak magnetic field, but not other key characteristics such as the small amplitude of harmonic components greater than 2 and the large

northward offset of the dipole (Heimpel et al., 2005; Stanley et al., 2005; Takahashi and Matsushima, 2006). On the other hand, models involving a stably stratified (i.e. non-convecting) layer at the top of the liquid core, with convection and dynamo action taking place beneath it, successfully predict a low-amplitude field with large dipolar and quadrupolar components (Christensen, 2006; Christensen and Wicht, 2008; Takahashi et al., 2019).

Core flow driven by a laterally-variable heat flux extracted at the base of the mantle has been identified as a potentially important ingredient to induce a stable dipolar field with a large quadrupolar component (Cao et al., 2014; Tian et al., 2015). Because of its 3:2 spin-orbit resonance, Mercury experiences an uneven insolation that results in large-scale differences of its surface temperature with cold poles at  $0^\circ$  and  $180^\circ$  latitude, and equatorial hot and warm poles at  $0^\circ$  and  $180^\circ$  and  $\pm 90^\circ$  longitude, respectively. Such pattern diffuses through the mantle leading to a high CMB heat flux at the poles (where the mantle is cooler) and a low heat flux in the equatorial regions (where the mantle is hotter) (Tosi et al., 2015). Cao et al. (2014), however, found that the characteristics of Mercury’s magnetic field are best reproduced when assuming the highest heat flux to be at the equator. Although such distribution could be important to constrain the planform of mantle convection, no obvious mechanism seems to be able to generate it and it is at odds with the heat flow pattern expected on the base of the surface temperature. The same holds for the degree-2 pattern postulated by Tian et al. (2015). The authors obtained a Mercury-like magnetic field assuming a high heat flux in the northern hemisphere, which they posited to be a remnant of the mantle activity that produced the northern volcanic plains 3.7–3.8 Ga (see Section 3). However, no mechanism has so far been proposed to generate hemispherical volcanism on Mercury and, at any rate, maintaining the required heat flux throughout Mercury’s evolution seems unlikely. Overall, a conclusive dynamo theory for Mercury and its link to the cooling mantle are yet to be established.

A low-altitude observation campaign carried out between 2014 and 2015 during the final phase of the mission, allowed MESSENGER to probe small-scale, low-amplitude magnetic fields of crustal origin. Johnson et al. (2015) identified a field with a peak intensity of about 20 nT in the Suisei Planitia region, consistent with the TRM of the underlying crust (Figure 5a). The analyzed region encompasses different geological units and, in particular, smooth volcanic plains emplaced between 3.9 and 3.7 Ga. Subsequent analyses revealed crustal magnetization associated with the Caloris and circum-Caloris region, which is of similar age (Hood, 2016). Overall, these observations indicate that a dynamo-generated field, most likely with a strength between that of the present-day field and up to a factor hundred higher (i.e. similar to the Earth’s) was active on Mercury at least until 3.7 Ga (Johnson et al., 2018). Models of the interior evolution of Mercury need thus to be compatible with an ancient dynamo active around 3.7 Ga as well as with the present-day one.

Whether or not a dynamo was active continuously throughout the planet’s history is unknown and represents a major source of uncertainty. Thermal evolution models of the interior of Mercury predict an initial phase of efficient crust production where the mantle heats up because of radiogenic heating (e.g., Tosi et al., 2013a; Padovan et al., 2017; Hauck et al., 2018). During this phase, the temperature difference between the mantle and core decreases and so does the heat flux at the CMB, which rapidly drops below the critical adiabatic value. A sub-adiabatic heat flux at the CMB—a common feature throughout most of the evolution of one-plate bodies—causes the top of the liquid core to become thermally stratified and suggests that thermal convection driven by mantle cooling alone can not be responsible for maintaining a dynamo over long time spans.

As for the cores of the other terrestrial planets, the composition of Mercury’s core is not well known. Dumberry and Rivoldini (2015) showed that under the assumption of a Fe-S composition, a present-day magnetic field together with geodetic constraints on Mercury’s moment of inertia and rotation state can be best accounted for if the inner core is relatively small ( $\leq 650$  km) and operates in the Fe-snow crystallization regime. However, a Fe-Si composition is thought to be more relevant for Mercury than a Fe-S one (Knibbe and van Westrenen, 2018). The low FeO content of the surface (Nittler et al., 2011) hints at reducing conditions for the mantle (Zolotov et al., 2013) which, during planet formation and core segregation, may have favoured the fractionation of Si rather than S in the core (e.g., Malavergne et al., 2010). In a crystallizing Fe-Si core, the amount of Si fractionating between solid and liquid is small (Kuwayama and Hirose, 2004). Upon freezing, negligible compositional buoyancy is generated,

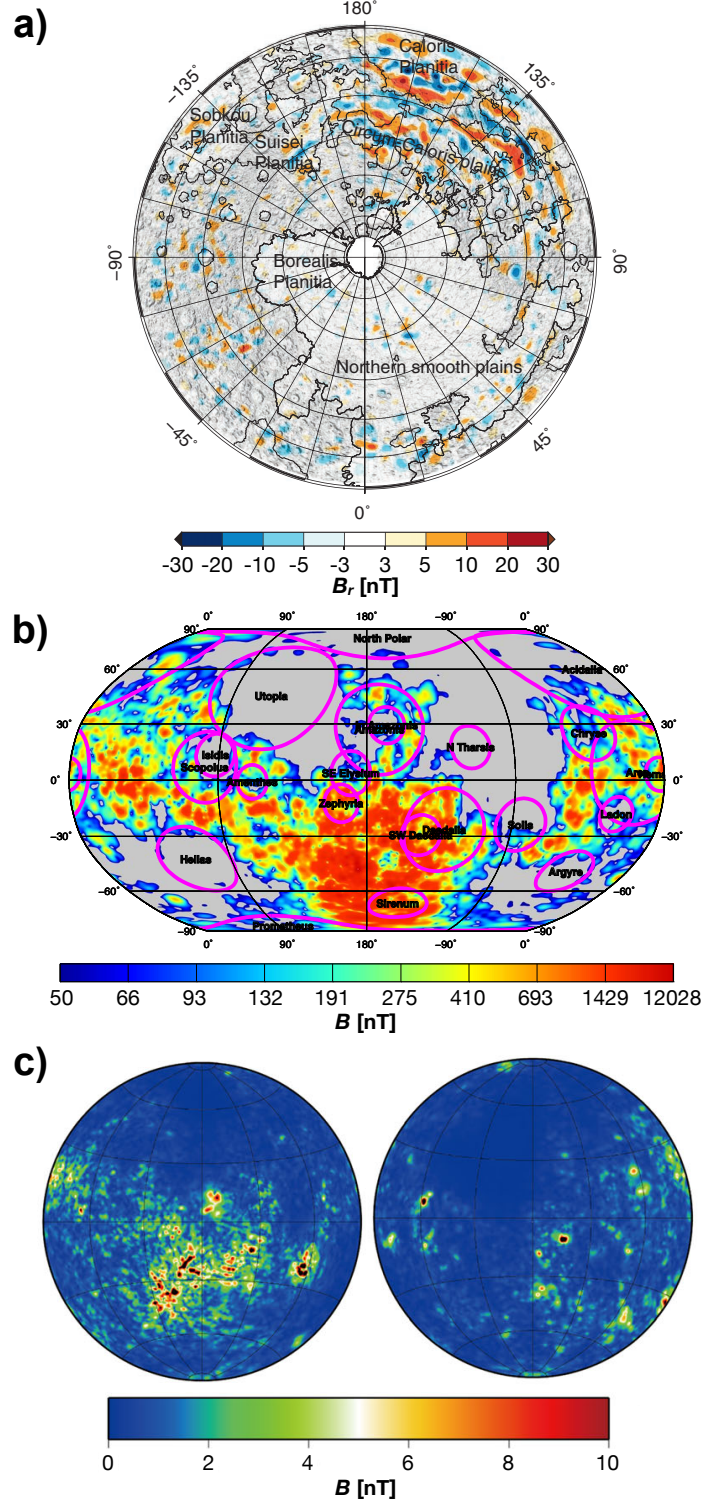


Figure 5: a) Map of the radial component of Mercury's magnetic field at 30 km altitude based on a model of lithospheric magnetization (from Johnson et al. (2018), Figure 5.19). b) Total intensity of the lithospheric magnetic field of Mars evaluated at the mean planetary radius of 3393.5 km. Thick purple circles indicate major impact basins (from Morschhauser (2016), Figure 10.8). c) Total intensity of the lithospheric magnetic field of the lunar nearside (left) and farside (right) at 30 km altitude (from Tsunakawa et al. (2015), Figure 2).

which thus can not drive core convection and dynamo action. In contrast to previous efforts largely based on the assumption of a Fe-S composition (Grott et al., 2011; Tosi et al., 2013a; Dumberry and Rivoldini, 2015), Knibbe and van Westrenen (2018) developed a model of Mercury's interior evolution including the crystallization of a Fe-Si core and, importantly, the self-consistent formation

of a thermally-stratified layer at the top of the liquid core caused by the expected drop of the mantle heat flux at the CMB in the early evolution. The authors showed that under these circumstances, core convection and an accompanying magnetic field can be powered by the release of latent heat (higher for a Fe-Si core than for a Fe-S one) within a thin liquid shell located between a liquid, but thermally-stratified, upper core, and a growing solid inner core. In agreement with the evidence of remnant crustal magnetization (Johnson et al., 2015), the model of Knibbe and van Westrenen (2018) also predicts an early onset of magnetic field generation, which is expected to continue until present due to the slow growth of the inner core.

## 5.2 Mars’ early magnetic field

At present, Mars does not possess a global-scale magnetic field of internal origin, but exhibits a strong, small-scale crustal magnetization largely associated with the old, heavily cratered southern highlands (e.g., Acuna et al., 1999) (Figure 5b). Therefore, a dynamo-generated field must have existed in the past. The lack of significant magnetization within large impact basins can be used to infer the time at which the Martian dynamo stopped operating. Impacts can reset the surface age as well as surface and crust magnetization over an area roughly corresponding to the size of the resulting crater (e.g., Mohit and Arkani-Hamed, 2004). The age of weakly- or non-magnetized basins provides thus an upper bound on the age of the dynamo and in turn a constraint for the thermal evolution of the interior. Analyses of the distribution of magnetization (or the lack thereof) of large basins together with the corresponding ages indicate that a dynamo stopped to be active on Mars before 4.0 – 4.1 Ga (e.g., Acuna et al., 1999; Lillis et al., 2008, 2013).

Most models of the thermal evolution of Mars’ interior, which can satisfy the above requirement of an early dynamo, consider this to be of thermal origin, i.e., powered by thermal convection in the core driven by a super-adiabatic CMB heat flux (e.g., Schubert and Spohn, 1990; Hauck and Phillips, 2002; Breuer and Spohn, 2003; Williams and Nimmo, 2004; Morschhauser et al., 2011; Samuel et al., 2019), although more speculative hypotheses such as that of a tidally-driven dynamo also exist (Arkani-Hamed, 2009). The required heat flux in excess of the core adiabatic gradient (eq. (6)) is easily obtained during the early evolution—for Mars as well as for other bodies—by simply considering the core to be initially super-heated with respect to the mantle, an expected outcome of core segregation (Solomon, 1979). This simple scenario is particularly plausible for Mars, which accreted and differentiated within the first few million years of the solar system (e.g., Nimmo and Kleine, 2007; Dauphas and Pourmand, 2011), a compressed timescale that likely prevented the interior from achieving thermal equilibration and favoured instead a large temperature difference between core and mantle.

Building on an early hypothesis of Sleep (1994), Nimmo and Stevenson (2000) argued that a strong heat flux at the CMB may have also been caused by cooling of the core due to plate tectonics operating during the first  $\sim 500$  Myr of Mars’ history and followed by a stagnant-lid regime that persisted until present. The reported discovery from Mars Global Surveyor data of alternating magnetic lineations in the southern hemisphere resembling those that characterize spreading oceanic ridges on Earth (Connerney et al., 2005) provided some observational ground to the hypothesis of early plate tectonics. However, the efficient mantle cooling initially caused by sinking plates tends to delay the subsequent production of crust once the stagnant lid regime is established because the sub-lithospheric mantle needs a relatively long time (1–2 Gyr) to heat up and produce partial melt (Breuer and Spohn, 2003). A delayed crust production is at odds with the evidence that volcanism and crust production on Mars were concentrated in the Noachian period (about 4.5 to 3.7 Ga) and declined since its end (see Section 3), thus making the plate tectonics hypothesis somewhat problematic.

While the generation of a thermal dynamo necessarily requires a sufficiently high CMB heat flux, its cessation may also be the result of large impacts (Roberts et al., 2009; Roberts and Arkani-Hamed, 2012, 2017; Monteux et al., 2015). The release of shock-pressure associated with impacts locally raises the mantle temperature and promotes the formation of upwellings beneath the impact region (see Section 4). As a consequence, the average heat flux at the base of the mantle tends to decrease. Several giant impacts likely occurred on Mars within a narrow time window ( $\sim 100$  Myr), around the time at which Mars’ global magnetic field disappeared (Frey, 2008; Frey and Mannoia, 2013).



Simulations of mantle convection including the (cumulative) thermal effects of impacts have shown that for events generating basins larger than 2500 km, the accompanying decrease of the CMB heat flux can be sufficient to stop the dynamo (Roberts and Arkani-Hamed, 2012). However, whether the dynamo is halted only temporarily or permanently, ultimately depends on the thermal state of the mantle preceding the impact as well as on its viscosity and thermal conductivity (Roberts and Arkani-Hamed, 2012, 2017), thus making it difficult to robustly evaluate this hypothesis.

### 5.3 The long-lived lunar magnetic field

Like Mars, the Moon lacks a present-day magnetic field, but it has been known since the Apollo era that lunar rocks and crust are magnetized (see, e.g. Fuller and Cisowski, 1987). Laboratory analyses of numerous Apollo samples show evidence of a paleomagnetic field from 4.25 Ga until possibly as recently as 200 Ma (see Weiss and Tikoo, 2014, for a review). However, the inferred field intensity varies widely among samples of different ages. Until 3.56 Ga, samples show a mean paleointensity of several tens of  $\mu\text{T}$  (e.g., Garrick-Bethell et al., 2009; Shea et al., 2012; Suavet et al., 2013). The intensity declines abruptly by about one order of magnitude around 3.2 – 3.3 Ga and remains at the level of few  $\mu\text{T}$  for younger samples. It has been recognized that due to the limited accuracy associated with the retrieval of the TRM of weakly magnetized samples, the low intensities inferred for samples younger than 3.3 Ga are actually compatible with a vanishingly small field (Tikoo et al., 2014; Buz et al., 2015). However, the recent measurements by Tikoo et al. (2017) appear sufficiently robust to indicate that a weak field of 5  $\mu\text{T}$  was indeed present at least 2.5 Ga, more likely around 1 Ga, firmly extending the lifetime of the lunar dynamo by about 1 to 2.5 billion years (based on the previous idea that 3.56 Ga was the youngest robust age of the dynamo). The actual time at which the dynamo ceased to operate remains unclear.

Accounting for a long-lived magnetic field of widely variable intensity poses a severe challenge for dynamo models. No single mechanism is able to account for an early, intense, and relatively short-lived dynamo between 4.25 and 3.56 Ga and a weak, long-lived one operating until (at least) 2.5 Ga and possibly longer. Several authors studied the conditions required to generate a magnetic dynamo on the Moon in the framework of coupled models of core-mantle evolution (e.g., Konrad and Spohn, 1997; Stegman et al., 2003; Evans et al., 2014; Laneuville et al., 2014; Scheinberg et al., 2015; Evans et al., 2018). A simple thermal dynamo induced by the cooling of a superheated core is generally possible only during the first few hundred million years of evolution for a chemically homogeneous mantle (e.g., Konrad and Spohn, 1997; Laneuville et al., 2014). A heat flux at the base of the mantle in excess of the core adiabatic heat flux can be maintained for a much longer time, even up to 2.5 Ga, in the presence of a compositionally-stratified mantle following the overturn of a crystallized magma ocean, particularly for a hydrous lower mantle where, upon overturn, water, behaving as incompatible, is sequestered within the deepest cumulates (Evans et al., 2014) (see Section 2). Considering, in addition to thermal buoyancy, the compositional buoyancy associated with the release of S upon core freezing (S is so far the only light alloying element considered in detail), easily extends the dynamo lifetime to billions of years (Laneuville et al., 2014; Scheinberg et al., 2015). A dynamo powered by core crystallization could even persist until present day unless a change in the regime of core crystallization from bottom-up to top-down takes place due to the progressive increase of S in the outer core (Laneuville et al., 2014; Rückriemen et al., 2018).

Overall, these models show that the generation of a long-lived lunar dynamo can be explained in terms of the well-known mechanisms of thermal and compositional buoyancy in the core induced by convective mantle cooling. However, accounting for the inferred intensity of the resulting magnetic field—both for the early and the late dynamo—is much more difficult. This is usually computed on the base of scaling laws derived from numerical simulations that express the intensity of a dynamo-generated magnetic field at a planetary surface in terms of, among other parameters, the heat flux at the CMB (Christensen, 2010). As discussed by Evans et al. (2018), in principle, thermo-compositional convection in the core could power until a recent past a weak field of  $\leq 1.9 \mu\text{T}$ , not exactly as high as the 5  $\mu\text{T}$  inferred by Tikoo et al. (2017). However, it cannot provide enough energy to generate a magnetic field of tens of  $\mu\text{T}$  until 3.56 Ga, even under the most optimistic assumptions on poorly known parameters. Non-convective dynamos generated via mechanical stirring of the liquid core



induced by precession of the Moon’s spin axis (Dwyer et al., 2011) or other instabilities associated with precession, librations, or tides that could be triggered by large impacts (Le Bars et al., 2011) also fall short by about one order of magnitude in predicting the surface intensity of the lunar magnetic field. A higher intensity of up to few tens of  $\mu\text{T}$  and hence close to the observed values, as well as a long-lived field could be accounted for by a “silicate dynamo” (Ziegler and Stegman, 2013) generated in a basal magma ocean atop the lunar core (Scheinberg et al., 2018). As discussed in Section 2, upon overturn of a crystallized magma ocean, dense cumulates enriched in incompatible HPEs may sink at the base of the mantle (e.g., Yu et al., 2019) and heat up (Stegman et al., 2003; Zhang et al., 2013a). If their density and heat sources content are sufficiently large, a basal magma ocean can form (see e.g. Plesa et al., 2014, for a description of this process in the context of early Mars). Provided that the poorly known, high-temperature electrical conductivity of the overturned silicates is sufficiently large, Scheinberg et al. (2018) showed that the surface intensity of a magnetic field generated in a thick basal magma ocean could be marginally compatible with the observations, largely because the surface strength of the magnetic field is positively affected by the vicinity and large size of the convective region.

In synthesis, observational constraints provide a relatively clear picture of the evolution of the lunar magnetic field. Its interpretation, however, is non-trivial. No single mechanism of magnetic field generation is able to account for both the amplitude and the timing of the dynamo. A combination of different mechanisms such as thermal convection (in the core or in a magma ocean), compositional convection, or mechanically-driven instabilities acting at different times and possibly in concert could be key to explain the history of the lunar magnetic field in its entirety.

## 6 Additional surficial manifestation

We devote this section to a brief discussion of additional constraints that can be placed on the interior evolution of stagnant-lid bodies. These constraints are both heavily model-dependent and their bearing on the interior evolution is somewhat indirect. They include planetary contraction and expansion, surface heat flux, and thickness of the elastic lithosphere.

### 6.1 Global contraction and expansion

The thermal evolution of terrestrial bodies can be manifest in the geological record through extensional and contractional features such as grabens and thrust faults, which if interpreted as a global response to the changes in the overall thermal state of the body, testify to periods of warming and cooling, respectively. In fact, the radius change  $\Delta R$  of a planet due to thermal expansion and contraction can be expressed as (e.g., Solomon and Chaiken, 1976):

$$\Delta R = \frac{1}{R_p^2} \int_0^{R_p} \alpha \Delta T(r) r^2 dr, \quad (7)$$

where  $R_p$  is the planet radius,  $r$  the radial coordinate,  $\alpha$  the coefficient of thermal expansion, and  $\Delta T(r)$  the laterally-averaged temperature variation over a given time interval. In addition, internal differentiation can also contribute to global variations in the planetary radius. On the one hand, melting associated with the production of secondary crust can cause radial expansion because of the lower density of the residual mantle material depleted in the incompatible elements that are enriched in the crust. On the other hand, freezing of an inner core can cause additional contraction due to the higher density of the solid part of the core that is progressively depleted in light alloying elements (e.g., Grott et al., 2011; Tosi et al., 2013a).

The interpretation of compressive tectonic features in terms of global planetary contraction is well established. It consists in mapping such features over the entire surface and using displacement–length scaling properties of faults to estimate the amount of radial shortening experienced by a given body (e.g. Watters et al., 2004; Byrne et al., 2014; Nahm and Schultz, 2011; Watters et al., 2010). With a surface dominated by compressive tectonic landforms (e.g., Strom et al., 1975)—lobate scarps and wrinkle ridges—Mercury is the body for which this approach has been used most extensively. Current

estimates based on MESSENGER images suggest an overall contraction of up to 7 km (Byrne et al., 2014), with up to two additional kilometres that could be accommodated by elastic deformation prior to the formation of the observed faults (Klimczak, 2015). Furthermore, cross-cutting relationships between faults and impact craters indicate that global contraction on Mercury started early, about 3.9 Ga, and continued until present at a decreasing rate (Crane and Klimczak, 2017). Models of the thermal evolution of Mercury typically predict a short initial phase of mantle heating and expansion lasting  $\sim 1$  Gyr, followed by cooling leading to a cumulative amount of radial contraction that compares well with the available observations, although the onset time of contraction tends to be slightly overestimated and the contraction rate to be constant rather than declining (e.g., Tosi et al., 2013a; Knibbe and van Westrenen, 2018; Hauck et al., 2018).

Similar compilations of compressional features at a global scale have been obtained for Mars (e.g., Knapmeyer et al., 2006). When considering all contractional structures regardless of their age, Nahm and Schultz (2011) inferred a maximum radial shortening of up to 3.77 km, although, as for Mercury, the expected rate of contraction would not be constant with time when taking into account the ages of the tectonic features. As discussed by Nahm and Schultz (2011), the overall cooling predicted by thermal evolution models of Mars (e.g., Andrews-Hanna et al., 2008b) significantly overestimates the inferred amount of global contraction. However, the extensive volcanic resurfacing underwent by the planet during the Hesperian epoch (about 3.7 to 3.0 Ga) (e.g., Greeley and Schneid, 1991) may have buried older faults generated by contraction, which renders a direct comparison with thermal evolution models non-trivial. Indeed, in contrast to Mercury, for which global contraction is traditionally used as one of the primary observations to constrain the interior evolution of the planet, models of Mars generally rely on different sets of observables (e.g., Plesa et al., 2018; Samuel et al., 2019).

On the Moon, the exceptional quality of the gravity experiment of the GRAIL mission revealed ancient igneous intrusions, indicative of an early phase of expansion of few km (Andrews-Hanna et al., 2013; Elkins-Tanton and Bercovici, 2014). Apart from tectonic structures observed within the lunar maria and associated with loading of mare basalts, compressional lobate scarps are the most common features present on the farside. Their length and surface relief, however, are much smaller than those of Mercury and Mars, implying an amount of global contraction of less than 1 km (e.g., Watters and Johnson, 2010; Watters et al., 2010). Early (and strongly simplified) models starting from a cold, accretion-like interior underlying a shallow magma ocean could meet this tight constraint (e.g., Solomon and Chaiken, 1976). More recent and sophisticated ones based on 3D thermal convection predict at least 2–3 km of shortening after an initial expansion phase (Zhang et al., 2013b; Rolf et al., 2016), which could be marginally compatible with the observations if additional contraction—up to 1.4 km according to Klimczak (2015)—was accumulated elastically without surface manifestation.

## 6.2 Heat flux and elastic lithosphere thickness

The heat flowing through the surface from the interior provides the most direct way to probe the thermal state of a planetary body. However, heat flux measurements on an extraterrestrial body currently exist only for the Moon (Langseth et al., 1976). Taken as part of the Apollo 15 and 17 missions, these measurements were conducted near the margins of the anomalous PKT region (Section 3). Even if they cannot be considered to be representative of the average lunar heat flux, they can still be used as a direct constraint for the global evolution of the interior (Laneuville et al., 2013; Laneuville et al., 2018).

As part of the InSight mission to Mars (Banerdt and Russell, 2017), the Heat Flow and Physical Properties Package (HP<sup>3</sup>), consisting of a self-hammering probe designed to measure the thermal conductivity and temperature gradient—hence the heat flux—across up to 5 m of Martian ground, was deployed on the surface of Mars on February 2019. As of July 2019, HP<sup>3</sup> has reached a depth of about 30 cm, still a small fraction of the minimum of 3 m necessary to perform a reliable heat flux estimate.

In the absence of direct measurements, the heat flux at a specific location can be inferred by estimating the effective thickness of the elastic lithosphere ( $T_e$ ) using gravity and topography data. Topographic features associated with observed gravity anomalies can either be compensated and hence in isostatic equilibrium in the presence of a strengthless lithosphere (e.g., Padovan et al., 2015), or

supported, partly or fully, by a lithosphere of finite strength. Although the crust-lithosphere system is characterized by a complex rheology, its flexural behavior can be approximated with that of an elastic plate overlying a strengthless interior. By making (rather strong) assumptions on the rheological properties of the crust and lithosphere and under the approximation of small plate curvature,  $T_e$  can be derived (McNutt, 1984) and further identified with the depth of a characteristic isotherm, thereby providing clues on the thermal gradient at specific locations. Furthermore, if the age of the topographic feature responsible for lithospheric flexure is also known, for example through crater counting, an attempt can be made to reconstruct the cooling history of the mantle by estimating  $T_e$  for features of different ages. Upon mantle cooling, the depth of the isotherm corresponding to  $T_e$  will increase and so the elastic thickness, thus indicating a heat flux that progressively decreases over the evolution.

In addition to the above inferences based on the use of gravity and topography data, the thickness of the elastic lithosphere beneath impact basins can be determined from loading and flexure models constrained by the distribution of tectonic structures within the basin (e.g., Comer et al., 1979; Solomon and Head, 1980), or from models of viscous or viscoelastic relaxation of the basin’s topographic relief (e.g., Solomon et al., 1982; Mohit and Phillips, 2006; Kamata et al., 2015), two approaches that have been extensively applied to the Moon.

For Mercury, only few estimates of the elastic thickness pertaining the early evolution are available (Melosh and McKinnon, 1988; Nimmo and Watters, 2004; Tosi et al., 2015; James et al., 2016). However, these are highly discordant, with values ranging from  $\sim 30 - 35$  km (Nimmo and Watters, 2004; James et al., 2016) to  $\sim 80 - 100$  km (Melosh and McKinnon, 1988; Tosi et al., 2015) around 3.9 – 3.8 Ga. The reasons of the discrepancy are not fully clear (Phillips et al., 2018), but possibly due to the different methods employed and approximations used to relate  $T_e$  with the internal temperature.

For the Moon, a variety of estimates have been made, mostly associated with impact basins. Values of  $T_e$  of less than 30 km have been suggested for basins older than 3.9 Ga (e.g., Kamata et al., 2015), possibly as small as 12 km (Crosby and McKenzie, 2005), suggesting an initially thin lithosphere and hot interior as expected for a mantle that crystallized from a magma ocean. For younger basins such as Crisium and Imbrium, a  $T_e$  of up to 75 km has been proposed (Solomon and Head, 1980), in line with the idea of rapidly thickening lithosphere in a cooling mantle.

From the analysis of gravity and topography associated with a variety of structures across Mars’ surface (see e.g., Grott et al., 2013, for a thorough discussion of the evolution of  $T_e$  on Mars), a consistent scenario emerges with  $T_e < 25$  km during the Noachian epoch (4.5 to 3.7 Ga), between  $\sim 50$  and 150 km during the Hesperian (3.7 to 3.0 Ga) and Amazonian (age  $\leq 3$  Ga), though with very large temporal uncertainties, and as large as 300 km at present day beneath the northern polar cap (Phillips et al., 2008). Recently, Plesa et al. (2018) presented 3D models of Mars’ interior evolution using, among others, constraints on the elastic thickness. These models agree generally well with the above estimates. In particular, the requirement of a large  $T_e$  at present-day beneath the north pole poses a tight constraint, limiting the set of admissible models to those characterized by a mantle highly depleted in HPEs. In fact, a limited amount of heat sources causes the mantle to cool over the evolution to generate a sufficiently large lithosphere thickness at present.

## 7 Summary and outlook

Combining the various constraints and models described in the previous sections, it is possible to outline likely scenarios for the evolution of Mercury, the Moon, and Mars. Of course the picture is far from being complete, and this outlook provides a summary and indicates potential avenues for future improvements of our understanding of the evolution of stagnant-lid bodies.

All three bodies likely had a magma ocean phase followed by fractional crystallization of the mantle, which set the stage for the subsequent evolution. The primary crust on the Moon and its traces on Mercury provide direct support to this hypothesis. A rapid formation within the first few million years of the solar system and isotopic evidence from meteorites favor a magma ocean also for Mars. A global-scale overturn of the solid mantle—beneath the stagnant lid or involving the lid—due to the gravitational instability of FeO-rich cumulates is a direct consequence of fractional crystallization and

the most widely explored scenario. However, for a slowly solidifying magma ocean, as is possibly the case for Mars and most likely for the Moon, convection and mixing can start during solidification. Existing models of the long-term evolution of these bodies constrained by observations mostly rely on the assumption of a homogeneous mantle. The long-term consequences of the complex processes associated with magma ocean crystallization are receiving more and more attention but are yet to be explored in detail for each planet.

The presence of the stagnant lid early on in the evolution (possibly following a brief episode of surface mobilization at the end of the magma ocean phase) causes inefficient heat loss, and hence heating and expansion of the mantle (Figure 6a), and crust formation (Figure 6b). The segregation of HPEs due to the formation of the primary crust of the Moon left the mantle largely depleted, which strongly limited the production of large volumes of secondary crust, but not of volcanism in general, as the lunar maria clearly show. The crusts of Mercury and Mars are instead mostly volcanic (i.e., secondary) and grew to the thickness inferred at present day from gravity and topography data within the first few hundred million years of evolution due to the production of partial melt, implying that a substantial amount of HPEs remained available to drive mantle convection and decompression melting after magma ocean solidification.

The phase of mantle heating and crust production is followed by secular cooling (Figure 6a), radial contraction, and by the increase of the thickness of the lithosphere and its elastic part. Surficial evidence is provided by the extent and number of compressive tectonic features, which allow the amount of radial contraction accumulated through a planet's history to be estimated. Such features are present on all the three bodies, particularly on Mercury, whose estimated contraction of about 7 km can be matched by evolution models. The smaller global contraction of Mars ( $< 4$  km) and the Moon ( $< 1$  km) are generally difficult to match by evolution models, which instead predict larger values, thus suggesting that part of the accumulated contraction may have been stored elastically with no surface expression. The effective elastic lithosphere thickness, estimated at specific locations by combining gravity and topography data with flexure modelling, increases with time due to mantle cooling. This behavior has been mostly recognized for Mars and is confirmed by numerical models. Large uncertainties associated with dating of the corresponding surface units somehow limit the use of this constraint.

In the early phases of the solar system many large objects collided with the newly formed planets, and the history of this tumultuous past is manifest in the battered surfaces of Mercury, the Moon, and to a somewhat lesser extent, Mars. The energies involved in this kind of events are extremely large, enough to interact with mantle convection, thus affecting the overall evolution, with melting activity, thus affecting the secondary crust production, and possibly with the core heat flux, thus affecting dynamo action. The most energetic events occur early on, and their dating is often quite uncertain, making the connection between these exogenous events and the interior processes they may interact with not straightforward to assess. However, it is clear that the mutual interaction depends on the interior thermal state, and, as such, large impact basins provide a window into the interior processes at the time of impact. There is evidence that the formation of the several large Martian basins did temporally stop dynamo action in the mantle, and that the properties of large lunar basins confirm the existence of large scale compositional heterogeneities in the mantle of the Moon. Compared to Mars and the Moon, data for Mercury are relatively sparse. However, as in the case of the Moon, the properties of its large basins are compatible with the overall evolution of the planet, as inferred from the entire set of available constraints (Figure 6).

Although at present-day only Mercury possesses a global magnetic field, an early one was active on all the three bodies, as the magnetization of their crust and lithosphere demonstrates (Figure 5). Thermal dynamos driven by a super-adiabatic heat flux extracted from the core by the convecting mantle are short-lived (Figure 6c). A thermal dynamo on Mercury would have likely stopped before 3.7 Ga (the age of the observed magnetized region). Furthermore, it is not known whether or not Mercury's magnetic field operated continuously from this age until present. Evolution models considering a core with Fe-Si composition and accounting for the effects of its crystallization seem to suggest so. An early episode of strong mantle and core cooling due to surface mobilization or to an initially hot core may have been responsible for the Martian dynamo, which ceased to operate  $\sim 4$  Ga. This mechanism

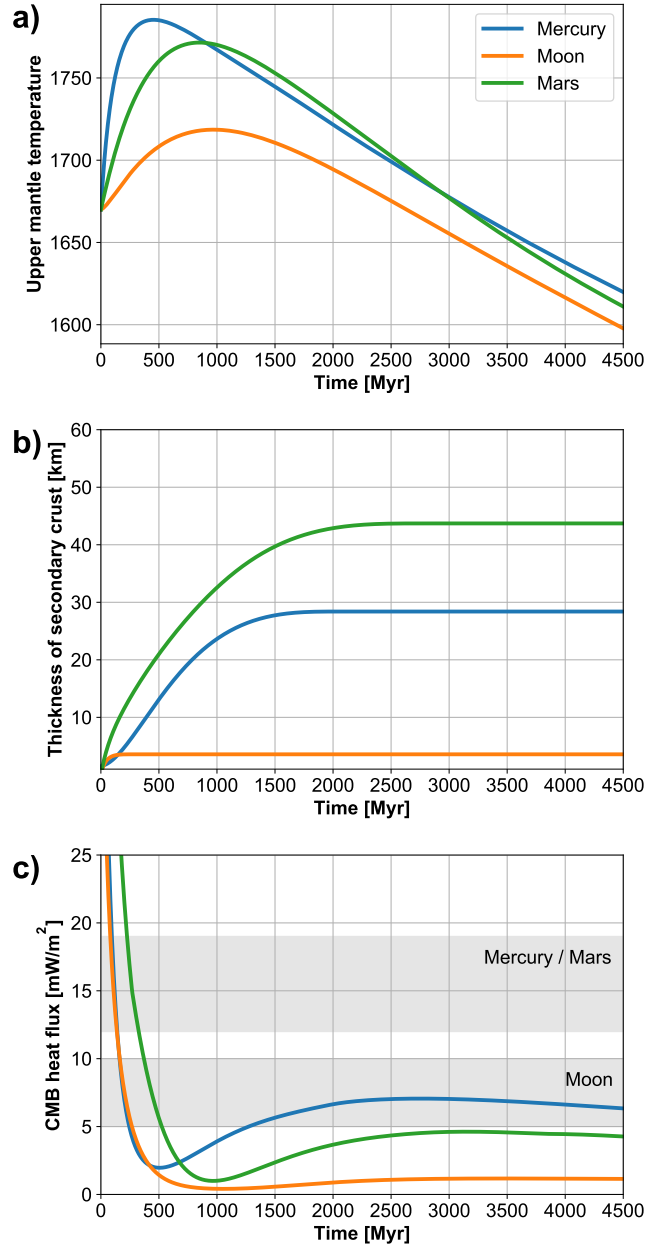


Figure 6: Possible evolution of the a) upper mantle temperature (i.e., the temperature beneath the stagnant lid), b) thickness of the secondary crust (which would sum up to an existing primary crust), and c) heat flux at the CMB for Mercury (blue lines), the Moon (orange lines), and Mars (green lines). In panel c, the two grey areas indicate a possible range of core adiabatic heat flux for Mercury and Mars (upper area between 12 and 19  $\text{mW/m}^2$ ), and for the Moon (lower area between 5 and 10  $\text{mW/m}^2$ ). The curves are obtained using parameterized thermal evolution models similar to those of Grott et al. (2013) and Tosi et al. (2013a), to which we refer for a complete description. Model parameters for Mercury are taken from Hauck et al. (2018), for Mars from Grott et al. (2013), and for the Moon from Laneuville et al. (2018).

is not sufficient to power the lunar dynamo, which survived until 2.5 Ga, possibly much longer, and generated  $\sim 4$  Ga a magnetic field of high intensity, which no single mechanism can account for.

The global evolutions of Mercury, the Moon and Mars illustrated in Figure 6 are valid for a specific model with a specific set of parameters. Yet, the figure shows that overall the evolution of the three bodies, as constrained by the observations described in this chapter, which are different for each body, is largely similar. Thus, one could surmise that thermal evolution models do capture the most important physical processes relevant to the thermo-chemical evolution of stagnant-lid bodies. However, given the large number of parameters that are required to run these kind of models (typically in excess of about 20), it is fair to admit that there is often enough room to adjust them in order to match the

observations. A better leverage on the predictive and inference powers of these models would require major advances along two main avenues: material properties and observational constraints. In terms of material properties we take viscosity as the most relevant example, since it represents a parameter that has a huge effect on the thermal evolution, but for which only very broad constraints exist. Viscosity is difficult to measure both in the laboratory and with theoretical calculations. Furthermore, in a planetary setting, it is affected by several poorly known and difficult to constrain factors, such as presence of melt, presence of volatiles, grain size, and dominant creep mechanism. These unavoidable obstacles imply that improvements in observational constraints are the most likely way to refine our understanding of the evolution of stagnant-lid bodies. With their potential ability of inferring interior structure, heat flux, crustal structure, and possibly density and temperature structures of the mantle, geophysical stations, such as the InSight lander currently located on the surface of Mars, are poised to provide a big step forward in our understanding of the detailed evolution history of the stagnant-lid bodies of the inner solar system. Complementary refinements of the dating of the surficial units, possible by direct analysis of samples, which will be facilitated by future sample return missions, will also improve the information content of a large set of additional constraints, from large basins properties to lid thickness estimates, which critically depend on the age of the associated crustal units.

It is somewhat self-evident that the level of complexity of a given model must depend on the detail, amount, and variety of the observations that the model is trying to explain. Future missions will provide new data, and evolution models will obviously need to be expanded and possibly adapted and tailored specifically for the different bodies. This future development will necessarily make the straightforward and informative comparison of the evolution of the different bodies, as presented in Figure 6, not possible. But this will only indicate that the field will have matured, which is only to be welcomed, as long as modelers will not attempt to reach the level of exactitude of the ancient Art of Cartography (Borges, 1999).

## Acknowledgments

We thank Maxim Ballmer for inviting us to write this manuscript and two anonymous reviewers for their comments that helped improve it. We also thank Maxime Maurice for his assistance in setting up the model used to generate Figure 1. N.T. acknowledges support by the Helmholtz Association (project VH-NG-1017) and S.P. by the DFG (Research Unit FOR 2440 Matter under planetary interior conditions).

## References

- Abe, Y. and Matsui, T. Early evolution of the Earth: Accretion, atmosphere formation, and thermal history. *J. Geophys. Res. Planets*, 91(B13):E291–E302, 1986. doi: 10.1029/JB091iB13p0E291.
- Acuna, M., Connerney, J., Lin, R., et al. Global distribution of crustal magnetization discovered by the Mars Global Surveyor MAG/ER experiment. *Science*, 284(5415):790–793, 1999.
- Anderson, B. J., Johnson, C. L., Korth, H., et al. Low-degree structure in Mercury’s planetary magnetic field. *J. Geophys. Res. Planets*, 117, 2012. doi: 10.1029/2012JE004159. URL 10.1029/2012JE004159.
- Andraut, D., Bolfan-Casanova, N., Nigro, G. L., et al. Solidus and liquidus profiles of chondritic mantle: Implication for melting of the Earth across its history. *Earth Planet. Sci. Lett.*, 304(1-2): 251–259, 2011. doi: 10.1016/j.epsl.2011.02.006.
- Andrews-Hanna, J. C., Zuber, M. T., and Banerdt, W. B. The Borealis basin and the origin of the martian crustal dichotomy. *Nature*, 453:1212–1215, 2008a. doi: 10.1038/nature07011.
- Andrews-Hanna, J. C., Zuber, M. T., and Hauck, S. A. Strike-slip faults on Mars: Observations and implications for global tectonics and geodynamics. *J. Geophys. Res. Planets*, 113(E8):E08002, 2008b. doi: 10.1029/2007JE002980.
- Andrews-Hanna, J. C., Asmar, S. W., Head, J. W., et al. Ancient igneous intrusions and early expansion of the moon revealed by grail gravity gradiometry. *Science*, 339(6120):675–678, 2013.
- Andrews-Hanna, J. C., Besserer, J., Head, I., James W., et al. Structure and evolution of the lunar Procellarum region as revealed by GRAIL gravity data. *Nature*, 514(7520):68–71, 2014. doi: 10.1038/nature13697.
- Arkani-Hamed, J. Did tidal deformation power the core dynamo of Mars? *Icarus*, 201(1):31–43, 2009. doi: 10.1016/j.icarus.2009.01.005.
- Ballmer, M. D., Lourenço, D. L., Hirose, K., Caracas, R., and Nomura, R. Reconciling magma-ocean crystallization models with the present-day structure of the Earth’s mantle. *Geochem. Geophys. Geosyst.*, 18(7):2785–2806, 2017. doi: 10.1002/2017GC006917.
- Banerdt, W. and Russell, C. Editorial on: Topical collection on insight mission to mars. *Space Sci. Rev.*, 211(1-4):1–3, 2017.
- Baratoux, D., Toplis, M., Monnereau, M., and Sautter, V. The petrological expression of early Mars volcanism. *J. Geophys. Res. Planets*, 118(1):59–64, 2013.
- Bibring, J.-P., Langevin, Y., Mustard, J. F., et al. Global Mineralogical and Aqueous Mars History Derived from OMEGA/Mars Express Data. *Science*, 312:400–404, 2006. doi: 10.1126/science.1122659.
- Bjorkman, M. D. and Holsapple, K. A. Velocity scaling impact melt volume. *Intern. J. Impact Engin.*, 5:155–163, 1987.
- Bland, M. T. and McKinnon, W. B. Mountain building on Io driven by deep faulting. *Nature Geosci.*, 9:429–432, 2016. doi: 10.1038/ngeo2711.
- Borges, J. L. *On Exactitude in Science*. In *Collected fictions*, The Penguin Press, 1999. Available at [kwarc.info/teaching/TDM/Borges.pdf](http://kwarc.info/teaching/TDM/Borges.pdf).
- Boukaré, C. E., Parmentier, E. M., and Parman, S. W. Timing of mantle overturn during magma ocean solidification. *Earth and Planetary Science Letters*, 491:216–225, 2018. doi: 10.1016/j.epsl.2018.03.037.

- Breuer, D. and Moore, W. B. Dynamics and thermal history of the terrestrial planets, the Moon, and Io. In Schubert, J., editor, *Planets and Moons* and edited by T. Spohn, *Treatise on Geophysics, Vol. 10*. Elsevier, Amsterdam, The Netherlands, 2<sup>nd</sup> edition, 2015.
- Breuer, D. and Spohn, T. Early plate tectonics versus single-plate tectonics on Mars: Evidence from magnetic field history and crust evolution. *J. Geophys. Res.*, 108(E7):5072, 2003. doi: 10.1029/2002JE001999.
- Breuer, D., Labrosse, S., and Spohn, T. Thermal evolution and magnetic field generation in terrestrial planets and satellites. *Space Sci. Rev.*, 152(1-4):449–500, 2010.
- Breuer, D., Rueckriemen, T., and Spohn, T. Iron snow, crystal floats, and inner-core growth: modes of core solidification and implications for dynamos in terrestrial planets and moons. *Prog. Earth Planet. Sci.*, 2:39, 2015. doi: 10.1186/s40645-015-0069-y.
- Brown, S. M. and Elkins-Tanton, L. T. Compositions of Mercury’s earliest crust from magma ocean models. *Earth Planet. Sc. Lett.*, 286:446–455, 2009. doi: 10.1016/j.epsl.2009.07.010.
- Buono, A. S. and Walker, D. The Fe-rich liquidus in the Fe-FeS system from 1 bar to 10 GPa. *Geochim. Cosmochim. Acta*, 75(8):2072–2087, 2011. doi: 10.1016/j.gca.2011.01.030.
- Buz, J., Weiss, B. P., Tikoo, S. M., et al. Magnetism of a very young lunar glass. *J. Geophys. Res. Planets*, 120(10):1720–1735, 2015. doi: 10.1002/2015JE004878.
- Byrne, P. K., Klimczak, C., Celâl Şengör, A. M., et al. Mercury’s global contraction much greater than earlier estimates. *Nat. Geosci.*, 7:301–307, 2014. doi: 10.1038/ngeo2097.
- Byrne, P. K., Ostrach, L. R., Fassett, C. I., et al. Widespread effusive volcanism on Mercury likely ended by about 3.5 Ga. *Geophys. Res. Lett.*, 43:7408–7416, 2016. doi: 10.1002/2016GL069412.
- Cadogan, P. H. Oldest and largest lunar basin? *Nature*, 250(5464):315–316, Jul 1974. doi: 10.1038/250315a0.
- Cao, H., Aurnou, J. M., Wicht, J., et al. A dynamo explanation for Mercury’s anomalous magnetic field. *Geophys. Res. Lett.*, 41(12):4127–4134, 2014. doi: 10.1002/2014GL060196.
- Carr, M. H. *The Surface of Mars*. Cambridge University Press, Cambridge, UK, 2006.
- Cassanelli, J. P. and Head, J. W. Did the Orientale impact melt sheet undergo large-scale igneous differentiation by crystal settling? *Geophys. Res. Lett.*, 43:11, 2016. doi: 10.1002/2016GL070425.
- Charlier, B., Grove, T. L., Namur, O., and Holtz, F. Crystallization of the lunar magma ocean and the primordial mantle-crust differentiation of the Moon. *Geochim. Cosmochim. Acta*, 234:50–69, 2018. doi: 10.1016/j.gca.2018.05.006.
- Chen, B., Li, J., and Hauck, S. A. Non-ideal liquidus curve in the Fe-S system and Mercury’s snowing core. *Geophys. Res. Lett.*, 35(7):L07201, 2008. doi: 10.1029/2008GL033311.
- Christensen, U. R. Dynamo Scaling Laws and Applications to the Planets. *Space Sci. Rev.*, 152(1-4): 565–590, 2010. doi: 10.1007/s11214-009-9553-2.
- Christensen, U. R. A deep dynamo generating Mercury’s magnetic field. *Nature*, 444(7122):1056–1058, 2006. doi: 10.1038/nature05342.
- Christensen, U. R. and Wicht, J. Models of magnetic field generation in partly stable planetary cores: Applications to Mercury and Saturn. *Icarus*, 196(1):16–34, 2008. doi: 10.1016/j.icarus.2008.02.013.
- Citron, R. I., Manga, M., and Tan, E. A hybrid origin of the Martian crustal dichotomy: Degree-1 convection antipodal to a giant impact. *Earth Planet. Sci. Lett.*, 491:58–66, 2018. doi: 10.1016/j.epsl.2018.03.031.



- Comer, R. P., Solomon, S. C., and Head, J. W. Elastic lithosphere thickness on the moon from mare tectonic features: a formal inversion. *Lun. Planet. Sci. Conf. Proc.*, 3:2441–2463, 1979.
- Connerney, J. E. P., Acuña, M. H., Ness, N. F., et al. Tectonic implications of Mars crustal magnetism. *Proc. Nat. Acad. Sci.*, 102(42):14970–14975, 2005. doi: 10.1073/pnas.0507469102.
- Costa, A., Caricchi, L., and Bagdassarov, N. A model for the rheology of particle-bearing suspensions and partially molten rocks. *Geochem. Geophys. Geosyst.*, 10(3):Q03010, 2009. doi: 10.1029/2008GC002138.
- Craddock, R. A. and Howard, A. D. The case for rainfall on a warm, wet early Mars. *J. Geophys. Res.*, 107:5111, 2002. doi: 10.1029/2001JE001505.
- Crane, K. T. and Klimczak, C. Timing and rate of global contraction on Mercury. *Geophys. Res. Lett.*, 44(7):3082–3089, 2017. doi: 10.1002/2017GL072711.
- Crosby, A. and McKenzie, D. Measurements of the elastic thickness under ancient lunar terrain. *Icarus*, 173(1):100–107, 2005. doi: 10.1016/j.icarus.2004.07.017.
- Dauphas, N. and Pourmand, A. Hf-W-Th evidence for rapid growth of Mars and its status as a planetary embryo. *Nature*, 473(7348):489–492, 2011. doi: 10.1038/nature10077.
- Davaille, A., Smrekar, S. E., and Tomlinson, S. Experimental and observational evidence for plume-induced subduction on Venus. *Nature Geosci.*, 10(5):349–355, 2017. doi: 10.1038/ngeo2928.
- Debaille, V., Brandon, A. D., O’Neill, C., Yin, Q. Z., and Jacobsen, B. Early martian mantle overturn inferred from isotopic composition of nakhlite meteorites. *Nat. Geosci.*, 2(8):548–552, 2009. doi: 10.1038/ngeo579.
- Denevi, B. W., Ernst, C. M., Meyer, H. M., et al. The distribution and origin of smooth plains on Mercury. *J. Geophys. Res. Planets*, 118:891–907, 2013. ISSN 2169-9100. doi: 10.1002/jgre.20075.
- Dumberry, M. and Rivoldini, A. Mercury’s inner core size and core-crystallization regime. *Icarus*, 248:254–268, 2015. doi: 10.1016/j.icarus.2014.10.038.
- Dwyer, C., Stevenson, D., and Nimmo, F. A long-lived lunar dynamo driven by continuous mechanical stirring. *Nature*, 479(7372):212, 2011.
- Elbeshausen, D. and Wünnemann, K. iSALE-3D: A three-dimensional, multi-material, multi-rheology hydrocode and its applications to large-scale geodynamic processes. In Schäfer, F. and Hiermaier, S., editors, *Proceedings of the 11th Hypervelocity Impact Symposium 2010*. Fraunhofer Verlag, 2011.
- Elkins-Tanton, L. T. Linked magma ocean solidification and atmospheric growth for Earth and Mars. *Earth Planet. Sci. Lett.*, 271(1-4):181–191, 2008. doi: 10.1016/j.epsl.2008.03.062.
- Elkins-Tanton, L. T. Magma Oceans in the Inner Solar System. *Ann. Rev. Earth Pl. Sc.*, 40:113–139, 2012. doi: 10.1146/annurev-earth-042711-105503.
- Elkins-Tanton, L. T. and Bercovici, D. Contraction or expansion of the Moon’s crust during magma ocean freezing? *Phil. Trans. Royal Soc. London Series A*, 372(2024):20130240–20130240, 2014. doi: 10.1098/rsta.2013.0240.
- Elkins-Tanton, L. T. and Hager, B. H. Giant meteoroid impacts can cause volcanism [rapid communication]. *Earth Planet. Sci. Lett.*, 239:219–232, 2005. doi: 10.1016/j.epsl.2005.07.029.
- Elkins-Tanton, L. T., Hager, B. H., and Grove, T. L. Magmatic effects of the lunar late heavy bombardment. *Earth Planet. Sci. Lett.*, 222:17–27, 2004. doi: 10.1016/j.epsl.2004.02.017.
- Elkins-Tanton, L. T., Zaranek, S. E., Parmentier, E. M., and Hess, P. C. Early magnetic field and magmatic activity on Mars from magma ocean cumulate overturn. *Earth Planet. Sci. Lett.*, 236(1-2):1–12, 2005. doi: 10.1016/j.epsl.2005.04.044.

- Elkins-Tanton, L. T., Parmentier, E., and Hess, P. Magma ocean fractional crystallization and cumulate overturn in terrestrial planets: Implications for Mars. *Meteorit. Planet. Sci.*, 38(12):1753–1771, 2003.
- Elkins-Tanton, L. T., Hess, P. C., and Parmentier, E. M. Possible formation of ancient crust on mars through magma ocean processes. *J. Geophys. Res.*, 110(E12), 2005. doi: 10.1029/2005JE002480.
- Elkins-Tanton, L. T., Burgess, S., and Yin, Q.-Z. The lunar magma ocean: Reconciling the solidification process with lunar petrology and geochronology. *Earth Planet. Sci. Lett.*, 304(3-4):326–336, 2011. doi: 10.1016/j.epsl.2011.02.004.
- Ernst, C. M., Denevi, B. W., Barnouin, O. S., et al. Stratigraphy of the Caloris basin, Mercury: Implications for volcanic history and basin impact melt. *Icarus*, 250:413–429, 2015. doi: 10.1016/j.icarus.2014.11.003.
- Evans, A. J., Zuber, M. T., Weiss, B. P., and Tikoo, S. M. A wet, heterogeneous lunar interior: Lower mantle and core dynamo evolution. *J. Geophys. Res. Planets*, 119(5):1061–1077, 2014. doi: 10.1002/2013JE004494.
- Evans, A. J., Tikoo, S. M., and Andrews-Hanna, J. C. The Case Against an Early Lunar Dynamo Powered by Core Convection. *Geophys. Res. Lett.*, 45(1):98–107, 2018. doi: 10.1002/2017GL075441.
- Fassett, C. I. Analysis of impact crater populations and the geochronology of planetary surfaces in the inner solar system. *J. Geophys. Res. Planets*, 121:1900–1926, 2016. doi: 10.1002/2016JE005094.
- Fassett, C. I., Head, J. W., Blewett, D. T., et al. Caloris impact basin: Exterior geomorphology, stratigraphy, morphometry, radial sculpture, and smooth plains deposits. *Earth Planet. Sci. Lett.*, 285:297–308, 2009. doi: 10.1016/j.epsl.2009.05.022.
- Fassett, C. I., Head, J. W., Baker, D. M. H., et al. Large impact basins on Mercury: Global distribution, characteristics, and modification history from MESSENGER orbital data. *J. Geophys. Res. Planets*, 117:E00L08, 2012. doi: 10.1029/2012JE004154.
- Fiquet, G., Auzende, A. L., Siebert, J., et al. Melting of Peridotite to 140 Gigapascals. *Science*, 329(5998):1516, 2010. doi: 10.1126/science.1192448.
- Foley, B. J., Bercovici, D., and Elkins-Tanton, L. T. Initiation of plate tectonics from post-magma ocean thermochemical convection. *J. Geophys. Res. Solid Earth*, 119(11):8538–8561, 2014. doi: 10.1002/2014JB011121.
- Frey, H. Ages of very large impact basins on mars: Implications for the late heavy bombardment in the inner solar system. *Geophys. Res. Lett.*, 35(13), 2008.
- Frey, H. and Mannoia, L. A revised, rated and dated inventory of very large candidate impact basins on Mars. In *Lun. Planet. Sci. Conf.*, volume 44, page 2501, 2013.
- Fuller, M. and Cisowski, S. M. Lunar paleomagnetism. In Jacobs, J. A., editor, *Geomagnetism*. Academic Press, Orlando, 1987.
- Garrick-Bethell, I. and Zuber, M. T. Elliptical structure of the lunar South Pole-Aitken basin. *Icarus*, 204(2):399–408, 2009. doi: 10.1016/j.icarus.2009.05.032.
- Garrick-Bethell, I., Weiss, B. P., Shuster, D. L., and Buz, J. Early Lunar Magnetism. *Science*, 323(5912):356, 2009. doi: 10.1126/science.1166804.
- Ghods, A. and Arkani-Hamed, J. Impact-induced convection as the main mechanism for formation of lunar mare basalts. *J. Geophys. Res. Planets*, 112:E03005, 2007. doi: 10.1029/2006JE002709.

- Golabek, G. J., Emsenhuber, A., Jutzi, M., Asphaug, E. I., and Gerya, T. V. Coupling SPH and thermochemical models of planets: Methodology and example of a Mars-sized body. *Icarus*, 301: 235–246, 2018. doi: 10.1016/j.icarus.2017.10.003.
- Golabek, G. J., Keller, T., Gerya, T. V., et al. Origin of the martian dichotomy and Tharsis from a giant impact causing massive magmatism. *Icarus*, 215(1):346–357, 2011. doi: 10.1016/j.icarus.2011.06.012.
- Greeley, R. and Schneid, B. D. Magma Generation on Mars: Amounts, Rates, and Comparisons with Earth, Moon, and Venus. *Science*, 254(5034):996–998, 1991. doi: 10.1126/science.254.5034.996.
- Grieve, R. A. Impact bombardment and its role in proto-continental growth on the early earth. *Precamb. Res.*, 10:217 – 247, 1980. ISSN 0301-9268. doi: [https://doi.org/10.1016/0301-9268\(80\)90013-3](https://doi.org/10.1016/0301-9268(80)90013-3).
- Grott, M., Breuer, D., and Laneuville, M. Thermo-chemical evolution and global contraction of mercury. *Earth Planet. Sc. Lett.*, 307:135–146, 2011. doi: 10.1016/j.epsl.2011.04.040.
- Grott, M., Baratoux, D., Hauber, E., et al. Long-Term Evolution of the Martian Crust-Mantle System. *Space Sci. Rev.*, 174(1-4):49–111, 2013. doi: 10.1007/s11214-012-9948-3.
- Hamano, K., Abe, Y., and Genda, H. Emergence of two types of terrestrial planet on solidification of magma ocean. *Nature*, 497(7451):607–610, 2013. doi: 10.1038/nature12163.
- Hartmann, W. K., Malin, M., McEwen, A., et al. Evidence for recent volcanism on Mars from crater counts. *Nature*, 397:586–589, 1999. doi: 10.1038/17545.
- Hauck, S. A., Grott, B. P. K., M., W., D. B., S., S., and J., M. T. Mercury’s global evolution. In Solomon, S. C., Anderson, B. J., and Nittler, L. R., editors, *Mercury, the view after MESSENGER*. Cambridge University Press, Cambridge, UK, 2018.
- Hauck, S. A., II, Margot, J.-L., Solomon, S. C., et al. The curious case of Mercury’s internal structure. *J. Geophys. Res. Planets*, 118:1204–1220, 2013. doi: 10.1002/jgre.20091.
- Hauck, S. A. and Phillips, R. J. Thermal and crustal evolution of Mars. *J. Geophys. Res. Planets*, 107(E7):5052, 2002. doi: 10.1029/2001JE001801.
- Hauck, S. A., Phillips, R. J., and Price, M. H. Venus: Crater distribution and plains resurfacing models. *J. Geophys. Res.*, 103(E6):13635–13642, 1998. doi: 10.1029/98JE00400.
- Head, J. W. and Wilson, L. Lunar mare volcanism: Stratigraphy, eruption conditions, and the evolution of secondary crusts. *Geochim. Cosmochim. Acta*, 56(6):2155–2175, 1992.
- Heimpel, M. H., Aurnou, J. M., Al-Shamali, F. M., and Gomez Perez, N. A numerical study of dynamo action as a function of spherical shell geometry. *Earth Planet. Sci. Lett.*, 236(1-2):542–557, 2005. doi: 10.1016/j.epsl.2005.04.032.
- Herrick, R. R. Resurfacing history of Venus. *Geology*, 22(8):703, 1994. doi: 10.1130/0091-7613.
- Hier-Majumder, S. and Hirschmann, M. M. The origin of volatiles in the Earth’s mantle. *Geochem. Geophys. Geosyst.*, 18(8):3078–3092, 2017. doi: 10.1002/2017GC006937.
- Hiesinger, H., Head, J., Wolf, U., Jaumann, R., and Neukum, G. Ages and stratigraphy of lunar mare basalts: A synthesis. *Recent Advances and Current Research Issues in Lunar Stratigraphy*, 477: 1–51, 2011.
- Holsapple, K. A. The Scaling of Impact Processes in Planetary Sciences. *Ann. Rev. Earth Planet. Sci.*, 21:333–373, 1993. doi: 10.1146/annurev.ea.21.050193.002001.

- Hood, L. L. Magnetic anomalies concentrated near and within Mercury’s impact basins: Early mapping and interpretation. *J. Geophys. Res. Planets*, 121(6):1016–1025, 2016. doi: 10.1002/2016JE005048.
- Ivanov, B. A. and Melosh, H. J. Impacts do not initiate volcanic eruptions: Eruptions close to the crater. *Geology*, 31:869, 2003. doi: 10.1130/G19669.1.
- James, P. B., Zuber, M. T., Phillips, R. J., and Solomon, S. C. Support of long-wavelength topography on Mercury inferred from MESSENGER measurements of gravity and topography. *J. Geophys. Res. Planets*, 120:287–310, 2015.
- James, P. B., Phillips, R. J., Grott, M., Hauck, S. A., and Solomon, S. C. The Thickness of Mercury’s Lithosphere Inferred from MESSENGER Gravity and Topography. In *Lun. Planet. Sci. Conf.*, page 1992, 2016.
- Johnson, C. L., Phillips, R. J., Purucker, M. E., et al. Low-altitude magnetic field measurements by MESSENGER reveal Mercury’s ancient crustal field. *Science*, 348:892–895, 2015. doi: 10.1126/science.aaa8720.
- Johnson, C. L., Anderson, B. J., Korth, H., Phillips, R. J., and Philipott, L. C. Mercury’s internal magnetic field. In Solomon, S. C., Anderson, B. J., and Nittler, L. R., editors, *Mercury, the view after MESSENGER*. Cambridge University Press, Cambridge, UK, 2018.
- Jolliff, B. L., Gillis, J. J., Haskin, L. A., Korotev, R. L., and Wieczorek, M. A. Major lunar crustal terranes: Surface expressions and crust-mantle origins. *J. Geophys. Res. Planets*, 105(E2):4197–4216, 2000.
- Jutzi, M. and Asphaug, E. Forming the lunar farside highlands by accretion of a companion moon. *Nature*, 476(7358):69–72, Aug 2011. doi: 10.1038/nature10289.
- Kamata, S., Sugita, S., Abe, Y., et al. The relative timing of Lunar Magma Ocean solidification and the Late Heavy Bombardment inferred from highly degraded impact basin structures. *Icarus*, 250: 492–503, 2015. doi: 10.1016/j.icarus.2014.12.025.
- Karki, B. B. and Stixrude, L. P. Viscosity of  $\text{MgSiO}_3$  Liquid at Earth’s Mantle Conditions: Implications for an Early Magma Ocean. *Science*, 328(5979):740, 2010. doi: 10.1126/science.1188327.
- Keller, T. and Tackley, P. J. Towards self-consistent modeling of the martian dichotomy: The influence of one-ridge convection on crustal thickness distribution. *Icarus*, 202(2):429–443, 2009. doi: 10.1016/j.icarus.2009.03.029.
- King, S. D. Venus Resurfacing Constrained by Geoid and Topography. *J. Geophys. Res. Planets*, 123(5):1041–1060, 2018. doi: 10.1002/2017JE005475.
- Klimczak, C. Limits on the brittle strength of planetary lithospheres undergoing global contraction. *J. Geophys. Res. Planets*, 120:2135–2151, 2015. doi: 10.1002/2015JE004851.
- Knapmeyer, M., Oberst, J., Hauber, E., et al. Working models for spatial distribution and level of Mars’ seismicity. *J. Geophys. Res.*, 111(E11):E11006, 2006. doi: 10.1029/2006JE002708.
- Knibbe, J. S. and van Westrenen, W. The thermal evolution of Mercury’s Fe-Si core. *Earth Planet. Sci. Lett.*, 482:147–159, 2018. doi: 10.1016/j.epsl.2017.11.006.
- Konrad, W. and Spohn, T. Thermal history of the Moon: implications for an early core dynamo and post-accretional magmatism. *Adv. Space Res.*, 19(10):1511–1521, 1997. doi: 10.1016/S0273-1177(97)00364-5.
- Kuwayama, Y. and Hirose, K. Phase relations in the system Fe-FeSi at 21 GPa. *Am. Mineral.*, 89(2-3):273–276, 2004. doi: 10.2138/am-2004-2-303.

- Labrosse, S., Hernlund, J. W., and Coltice, N. A crystallizing dense magma ocean at the base of the Earth’s mantle. *Nature*, 450:866–869, 2007. doi: 10.1038/nature06355.
- Labrosse, S., Morison, A., Deguen, R., and Alboussière, T. Rayleigh-Bénard convection in a creeping solid with melting and freezing at either or both its horizontal boundaries. *J. Fluid. Mech.*, 846: 5–36, 2018. doi: 10.1017/jfm.2018.258.
- Labrosse, S., Hernlund, J. W., and Hirose, K. Fractional melting and freezing in the deep mantle and implications for the formation of a basal magma ocean. In Badro, J. and Walter, M., editors, *The early Earth*, volume 212 of *Geophysical Monograph Series*, pages 123–142. Wiley, 2015. doi: 10.1002/9781118860359.ch7.
- Laneuville, M., Wieczorek, M., Breuer, D., and Tosi, N. Asymmetric thermal evolution of the moon. *J. Geophys. Res. Planets*, 118(7):1435–1452, 2013.
- Laneuville, M., Wieczorek, M., Breuer, D., et al. A long-lived lunar dynamo powered by core crystallization. *Earth Planet. Sci. Lett.*, 401:251–260, 2014.
- Laneuville, M., Taylor, J., and Wieczorek, M. A. Distribution of Radioactive Heat Sources and Thermal History of the Moon. *J. Geophys. Res. Planets*, 123(12):3144–3166, 2018. doi: 10.1029/2018JE005742.
- Langseth, M. G., Keihm, S. J., and Peters, K. Revised lunar heat-flow values. In *Lunar Planet. Sci. Conf.*, volume 7, pages 3143–3171, 1976.
- Lawrence, D. J., Feldman, W. C., Barraclough, B. L., et al. Global Elemental Maps of the Moon: The Lunar Prospector Gamma-Ray Spectrometer. *Science*, 281:1484, 1998. doi: 10.1126/science.281.5382.1484.
- Lawrence, D., Elphic, R., Feldman, W., et al. Small-area thorium features on the lunar surface. *J. Geophys. Res.*, 108(E9), 2003.
- Le Bars, M. Flows driven by libration, precession, and tides in planetary cores\*. *Phys. Rev. Fluids*, 1 (6):060505, 2016. doi: 10.1103/PhysRevFluids.1.060505.
- Le Bars, M., Wieczorek, M. A., Karatekin, Ö., Cébron, D., and Laneuville, M. An impact-driven dynamo for the early moon. *Nature*, 479(7372):215, 2011.
- Le Feuvre, M. and Wieczorek, M. A. Nonuniform cratering of the terrestrial planets. *Icarus*, 197: 291–306, 2008. doi: 10.1016/j.icarus.2008.04.011.
- Lebrun, T., Massol, H., Chassefière, E., et al. Thermal evolution of an early magma ocean in interaction with the atmosphere. *J. Geophys. Res. Planets*, 118(6):1155–1176, 2013. doi: 10.1002/jgre.20068.
- Li, H., Zhang, N., Liang, Y., et al. Lunar cumulate mantle overturn: A model constrained by ilmenite rheology. *J. Geophys. Res. Planets*, 2019.
- Lillis, R. J., Frey, H. V., and Manga, M. Rapid decrease in Martian crustal magnetization in the Noachian era: Implications for the dynamo and climate of early Mars. *Geophys. Res. Lett.*, 35(14): L14203, 2008. doi: 10.1029/2008GL034338.
- Lillis, R. J., Robbins, S., Manga, M., Halekas, J. S., and Frey, H. V. Time history of the Martian dynamo from crater magnetic field analysis. *J. Geophys. Res. Planets*, 118(7):1488–1511, 2013. doi: 10.1002/jgre.20105.
- Maas, C. and Hansen, U. Effects of Earth’s rotation on the early differentiation of a terrestrial magma ocean. *J. Geophys. Res. Solid Earth*, 120(11):7508–7525, 2015. doi: 10.1002/2015JB012053.
- Maas, C. and Hansen, U. Dynamics of a terrestrial magma ocean under planetary rotation: A study in spherical geometry. *Earth Planet. Sci. Lett.*, 513:81–94, 2019. doi: 10.1016/j.epsl.2019.02.016.

- Malavergne, V., Toplis, M. J., Berthet, S., and Jones, J. Highly reducing conditions during core formation on Mercury: Implications for internal structure and the origin of a magnetic field. *Icarus*, 206:199–209, 2010. doi: 10.1016/j.icarus.2009.09.001.
- Marchi, S., Mottola, S., Cremonese, G., Massironi, M., and Martellato, E. A New Chronology for the Moon and Mercury. *Astrophys. J.*, 137:4936–4948, 2009. doi: 10.1088/0004-6256/137/6/4936.
- Marchi, S., Chapman, C. R., Fassett, C. I., et al. Global resurfacing of Mercury 4.0–4.1 billion years ago by heavy bombardment and volcanism. *Nature*, 499:59–61, 2013. doi: 10.1038/nature12280.
- Marinova, M. M., Aharonson, O., and Asphaug, E. Mega-impact formation of the Mars hemispheric dichotomy. *Nature*, 453(7199):1216–1219, 2008. doi: 10.1038/nature07070.
- Maurice, M., Tosi, N., Samuel, H., et al. Onset of solid-state mantle convection and mixing during magma ocean solidification. *J. Geophys. Res. Planets*, 122(3):577–598, 2017. doi: 10.1002/2016JE005250.
- McEwen, A. S., Malin, M. C., Carr, M. H., and Hartmann, W. K. Voluminous volcanism on early Mars revealed in Valles Marineris. *Nature*, 397:584–586, 1999. doi: 10.1038/17539.
- McNutt, M. K. Lithospheric flexure and thermal anomalies. *J. Geophys. Res.*, 89:11180–11194, 1984. doi: 10.1029/JB089iB13p11180.
- Melosh, H. J. and McKinnon, W. B. The tectonics of Mercury. In Vilas, F., Chapman, C. R., & Matthews, M. S., editor, *Mercury*, pages 374–400. University of Arizona Press, 1988.
- Melosh, H. J., Freed, A. M., Johnson, B. C., et al. The Origin of Lunar Mascon Basins. *Science*, 340:1552–1555, 2013. doi: 10.1126/science.1235768.
- Melosh, H. J. *Impact cratering: A geologic process*. Oxford University Press (Oxford Monographs on Geology and Geophysics, No. 11), 1989, 253 p., 1989.
- Melosh, H. J. *Planetary surface processes*. Cambridge University Press, 2011.
- Meyer, J., Elkins-Tanton, L., and Wisdom, J. Coupled thermal-orbital evolution of the early Moon. *Icarus*, 208(1):1–10, 2010. doi: 10.1016/j.icarus.2010.01.029.
- Mezger, K., Debaille, V., and Kleine, T. Core Formation and Mantle Differentiation on Mars. *Space Sci. Rev.*, 174(1-4):27–48, 2013. doi: 10.1007/s11214-012-9935-8.
- Michael, G., Basilevsky, A., and Neukum, G. On the history of the early meteoritic bombardment of the Moon: Was there a terminal lunar cataclysm? *Icarus*, 302:80 – 103, 2018. ISSN 0019-1035. doi: <https://doi.org/10.1016/j.icarus.2017.10.046>.
- Miljković, K., Wieczorek, M. A., Collins, G. S., et al. Asymmetric distribution of lunar impact basins caused by variations in target properties. *Science*, 342:724–726, 2013. doi: 10.1126/science.1243224. URL <http://www.sciencemag.org/content/342/6159/724.abstract>.
- Mohit, P. S. and Phillips, R. J. Viscoelastic evolution of lunar multiring basins. *J. Geophys. Res. Planets*, 111(E12):E12001, 2006. doi: 10.1029/2005JE002654.
- Mohit, P. S. and Arkani-Hamed, J. Impact demagnetization of the martian crust. *Icarus*, 168(2):305–317, 2004. doi: 10.1016/j.icarus.2003.12.005.
- Monaghan, J. J. Smoothed particle hydrodynamics. *Ann. Rev. Astron. Astrophys.*, 30:543–574, 1992. doi: 10.1146/annurev.aa.30.090192.002551.
- Monteux, J., Andraut, D., and Samuel, H. On the cooling of a deep terrestrial magma ocean. *Earth Planet. Sci. Lett.*, 448:140–149, 2016. doi: 10.1016/j.epsl.2016.05.010.

- Monteux, J., Amit, H., Choblet, G., Langlais, B., and Tobie, G. Giant impacts, heterogeneous mantle heating and a past hemispheric dynamo on Mars. *Phys. Earth Planet. Int.*, 240:114–124, 2015. doi: 10.1016/j.pepi.2014.12.005.
- Moore, W. B. and Schubert, G. The tidal response of Ganymede and Callisto with and without liquid water oceans. *Icarus*, 166:223–226, 2003. doi: 10.1016/j.icarus.2003.07.001.
- Moore, W. B. and Webb, A. A. G. Heat-pipe Earth. *Nature*, 501(7468):501–505, 2013. doi: 10.1038/nature12473.
- Morbidelli, A., Bottke, W. F., Jr., Froeschlé, C., and Michel, P. Origin and Evolution of Near-Earth Objects. In Bottke, W. F., Jr., Cellino, A., Paolicchi, P., and Binzel, R. P., editors, *Asteroids III*, pages 409–422. University of Arizona Press, 2002.
- Morbidelli, A., Marchi, S., Bottke, W. F., and Kring, D. A. A sawtooth-like timeline for the first billion years of lunar bombardment. *Earth Planet. Sci. Lett.*, 355:144–151, 2012. doi: 10.1016/j.epsl.2012.07.037.
- Morbidelli, A., Nesvorný, D., Laurenz, V., et al. The timeline of the lunar bombardment: Revisited. *Icarus*, 305:262–276, 2018. doi: 10.1016/j.icarus.2017.12.046.
- Morison, A., Labrosse, S., Deguen, R., and Alboussière, T. Timescale of overturn in a magma ocean cumulate. *Earth Planet. Sci. Lett.*, 516:25–36, 2019. doi: 10.1016/j.epsl.2019.03.037.
- Morschhauser, A. *A model of the crustal magnetic field of Mars*. PhD thesis, Westfälischen Wilhelms-Universität Münster, Münster, March 2016. 187 pp.
- Morschhauser, A., Grott, M., and Breuer, D. Crustal recycling, mantle dehydration, and the thermal evolution of Mars. *Icarus*, 212:541–558, 2011. doi: 10.1016/j.icarus.2010.12.028.
- Murchie, S. L., Klima, R. L., Denevi, B. W., et al. Orbital multispectral mapping of Mercury with the MESSENGER Mercury Dual Imaging System: Evidence for the origins of plains units and low-reflectance material. *Icarus*, 254:287–305, 2015. doi: 10.1016/j.icarus.2015.03.027.
- Nahm, A. L. and Schultz, R. A. Magnitude of global contraction on Mars from analysis of surface faults: Implications for martian thermal history. *Icarus*, 211(1):389–400, 2011.
- Nakagawa, T. and Tackley, P. J. Influence of plate tectonic mode on the coupled thermochemical evolution of Earth’s mantle and core. *Geochem. Geophys. Geosyst.*, 16(10):3400–3413, 2015. doi: 10.1002/2015GC005996.
- Namur, O., Collinet, M., Charlier, B., et al. Melting processes and mantle sources of lavas on Mercury. *Earth Planet. Sc. Lett.*, 439:117–128, 2016. doi: 10.1016/j.epsl.2016.01.030.
- Neukum, G. and Ivanov, B. A. Crater size distributions and impact probabilities on earth from lunar, terrestrial-planet, and asteroid cratering data. In Gehrels, T., editor, *Hazards due to comets and asteroids*, pages 359 – 416. Univ. Arizona Press, 1994.
- Neukum, G., Jaumann, R., Hoffmann, H., et al. Recent and episodic volcanic and glacial activity on Mars revealed by the High Resolution Stereo Camera. *Nature*, 432(7020):971–979, 2004. doi: 10.1038/nature03231.
- Neumann, G. A., Zuber, M. T., Wieczorek, M. A., et al. Crustal structure of Mars from gravity and topography. *J. Geophys. Res. Planets*, 109(E8):E08002, 2004. doi: 10.1029/2004JE002262.
- Nikolaou, A., Katyal, N., Tosi, N., et al. What Factors Affect the Duration and Outgassing of the Terrestrial Magma Ocean? *Astrophys. J.*, 875(1):11, 2019. doi: 10.3847/1538-4357/ab08ed.
- Nimmo, F. and Kleine, T. How rapidly did Mars accrete? Uncertainties in the Hf W timing of core formation. *Icarus*, 191(2):497–504, 2007. doi: 10.1016/j.icarus.2007.05.002.

- Nimmo, F. and Stevenson, D. Influence of early plate tectonics on the thermal evolution and magnetic field of mars. *J. Geophys. Res.*, 105(E5):11969–11979, 2000.
- Nimmo, F. and Watters, T. R. Depth of faulting on Mercury: Implications for heat flux and crustal and effective elastic thickness. *Geophys. Res. Lett.*, 31:L02701, 2004. doi: 10.1029/2003GL018847.
- Nimmo, F. and Tanaka, K. Early crustal evolution of mars. *Annu. Rev. Earth Planet. Sci.*, 33: 133–161, 2005.
- Nittler, L. R., Starr, R. D., Weider, S. Z., et al. The major-element composition of Mercury’s surface from MESSENGER X-ray spectrometry. *Science*, 333:1847–1850, 2011. doi: 10.1126/science.1211567.
- Nittler, L. R., Chabot, N. L., Grove, T. L., and Peplowski, P. N. The Chemical Composition of Mercury. In Solomon, S. C., Anderson, B. J., and Nittler, L. R., editors, *Mercury, the view after MESSENGER*. Cambridge University Press, Cambridge, UK, 2018.
- Olson, P. Planetary magnetism. In Cardin, P. and Cugliandolo, L., editors, *Dynamos - Lecture Notes of the Les Houches Summer School 2007*, pages 137–249. Elsevier, 2008.
- O’Reilly, T. C. and Davies, G. F. Magma transport of heat on Io: A mechanism allowing a thick lithosphere. *Geophys. Res. Lett.*, 8(4):313–316, 1981. doi: 10.1029/GL008i004p00313.
- Padovan, S., Wieczorek, M. A., Margot, J.-L., Tosi, N., and Solomon, S. C. Thickness of the crust of Mercury from geoid-to-topography ratios. *Geophys. Res. Lett.*, 42(4):1029–1038, 2015. doi: 10.1002/2014GL062487.
- Padovan, S., Tosi, N., Plesa, A.-C., and Ruedas, T. Impact-induced changes in source depth and volume of magmatism on Mercury and their observational signatures. *Nature Comm.*, 8:1945, 2017. doi: 10.1038/s41467-017-01692-0.
- Paige, D. and Siegler, M. New constraints on lunar heat flow rates from lro diviner lunar radiometer experiment polar observations. In *Lunar Planet. Sci. Conf.*, volume 47, page 2753, 2016.
- Parmentier, E., Zhong, S., and Zuber, M. Gravitational differentiation due to initial chemical stratification: origin of lunar asymmetry by the creep of dense creep? *Earth Planet. Sci. Lett.*, 201(3-4): 473–480, 2002.
- Peale, S. J., Cassen, P., and Reynolds, R. T. Melting of Io by tidal dissipation. *Science*, 203:892–894, 1979. doi: 10.1126/science.203.4383.892.
- Peplowski, P. N., Klima, R. L., Lawrence, D. J., et al. Remote sensing evidence for an ancient carbon-bearing crust on Mercury. *Nature Geosci.*, 9(4):273–276, 2016. doi: 10.1038/ngeo2669.
- Perera, V., Jackson, A. P., Elkins-Tanton, L. T., and Asphaug, E. Effect of reimpacting debris on the solidification of the lunar magma ocean. *J. Geophys. Res. Planets*, 123(5):1168–1191, 2018.
- Perry, M. E., Neumann, G. A., Phillips, R. J., et al. The low-degree shape of Mercury. *Geophys. Res. Lett.*, 42:6951–6958, 2015. doi: 10.1002/2015GL065101.
- Phillips, R. J., Byrne, P. K., James, P. B., et al. Mercury’s crust and lithosphere: Structure and mechanics. In Solomon, S. C., Anderson, B. J., and Nittler, L. R., editors, *Mercury, the view after MESSENGER*. Cambridge University Press, Cambridge, UK, 2018.
- Phillips, R. J., Zuber, M. T., Smrekar, S. E., et al. Mars North Polar Deposits: Stratigraphy, Age, and Geodynamical Response. *Science*, 320(5880):1182, 2008. doi: 10.1126/science.1157546.
- Pierazzo, E., Vickery, A. M., and Melosh, H. J. A reevaluation of impact melt production. *Icarus*, 127:408–423, 1997. doi: 10.1006/icar.1997.5713.



- Plesa, A.-C., Tosi, N., and Breuer, D. Can a fractionally crystallized magma ocean explain the thermochemical evolution of Mars? *Earth Planet. Sci. Lett.*, 403:225–235, 2014. doi: 10.1016/j.epsl.2014.06.034.
- Plesa, A.-C., Grott, M., Tosi, N., et al. How large are present-day heat flux variations across the surface of mars? *J. Geophys. Res. Planets*, 121(12):2386–2403, 2016.
- Plesa, A.-C., Padovan, S., Tosi, N., et al. The Thermal State and Interior Structure of Mars. *Geophys. Res. Lett.*, 45:12, 2018. doi: 10.1029/2018GL080728.
- Potter, R. W. K., Collins, G. S., Kiefer, W. S., McGovern, P. J., and Kring, D. A. Constraining the size of the South Pole-Aitken basin impact. *Icarus*, 220:730–743, 2012. doi: 10.1016/j.icarus.2012.05.032.
- Press, F. and Siever, R. *Earth*. Freeman and Company, San Francisco, 1978.
- Rampino, M. R. Impact cratering and flood basalt volcanism. *Nature*, 327(6122):468, 1987.
- Reese, C. C. and Solomatov, V. S. Fluid dynamics of local martian magma oceans. *Icarus*, 184:102–120, 2006. doi: 10.1016/j.icarus.2006.04.008.
- Reese, C. C., Solomatov, V. S., and Baumgardner, J. R. Survival of impact-induced thermal anomalies in the Martian mantle. *J. Geophys. Res.*, 107:5082, 2002. doi: 10.1029/2000JE001474.
- Reese, C. C., Solomatov, V. S., Baumgardner, J. R., Stegman, D. R., and Vezolainen, A. V. Magmatic evolution of impact-induced Martian mantle plumes and the origin of Tharsis. *J. Geophys. Res.*, 109:E08009, 2004. doi: 10.1029/2003JE002222.
- Roberts, J. H. and Arkani-Hamed, J. Impact-induced mantle dynamics on Mars. *Icarus*, 218:278–289, 2012. doi: 10.1016/j.icarus.2011.11.038.
- Roberts, J. H. and Arkani-Hamed, J. Effects of basin-forming impacts on the thermal evolution and magnetic field of Mars. *Earth Planet. Sci. Lett.*, 478:192–202, 2017. doi: 10.1016/j.epsl.2017.08.031.
- Roberts, J. H. and Barnouin, O. S. The effect of the Caloris impact on the mantle dynamics and volcanism of Mercury. *J. Geophys. Res. Planets*, 117:E02007, 2012. doi: 10.1029/2011JE003876.
- Roberts, J. H., Lillis, R. J., and Manga, M. Giant impacts on early Mars and the cessation of the Martian dynamo. *J. Geophys. Res. Planets*, 114(E4):E04009, 2009. doi: 10.1029/2008JE003287.
- Roberts, J. H. and Zhong, S. Degree-1 convection in the Martian mantle and the origin of the hemispheric dichotomy. *J. Geophys. Res. Planets*, 111(E6):E06013, 2006. doi: 10.1029/2005JE002668.
- Robinson, M. S., Murchie, S. L., Blewett, D. T., et al. Reflectance and color variations on Mercury: Regolith processes and compositional heterogeneity. *Science*, 321(5885):66, 2008. doi: 10.1126/science.1160080.
- Rogers, G. C. Oceanic plateaus as meteorite impact signatures. *Nature*, 299:341–342, 1982. doi: 10.1038/299341a0.
- Rolf, T., Zhu, M.-H., Wünnemann, K., and Werner, S. C. The role of impact bombardment history in lunar evolution. *Icarus*, 286:138–152, 2016. doi: 10.1016/j.icarus.2016.0.007.
- Rolf, T., Steinberger, B., Sruthi, U., and Werner, S. C. Inferences on the mantle viscosity structure and the post-overtake evolutionary state of Venus. *Icarus*, 313:107–123, 2018. doi: 10.1016/j.icarus.2018.05.014.
- Ronca, L. B. Meteoritic impact and volcanism. *Icarus*, 5:515–520, 1966. doi: 10.1016/0019-1035(66)90063-7.
- Rückriemen, T., Breuer, D., and Spohn, T. Top-down freezing in a Fe-FeS core and Ganymede’s present-day magnetic field. *Icarus*, 307:172–196, 2018. doi: 10.1016/j.icarus.2018.02.021.

- Ruedas, T. and Breuer, D. “Isocrater” impacts: Conditions and mantle dynamical responses for different impactor types. *Icarus*, 306:94–115, 2018. doi: 10.1016/j.icarus.2018.02.005.
- Ruedas, T. and Breuer, D. Dynamical effects of multiple impacts: Large impacts on a mars-like planet. *Phys. Earth Planet. Int.*, 287:76–92, 2019.
- Salvador, A., Massol, H., Davaille, A., et al. The relative influence of H<sub>2</sub>O and CO<sub>2</sub> on the primitive surface conditions and evolution of rocky planets. *J. Geophys. Res. Planets*, 122(7):1458–1486, 2017. doi: 10.1002/2017JE005286.
- Samuel, H., Lognonné, P., Panning, M., and Lainey, V. The rheology and thermal history of Mars revealed by the orbital evolution of Phobos. *Nature*, 569(7757):523–527, 2019. doi: 10.1038/s41586-019-1202-7.
- Scheinberg, A., Elkins-Tanton, L. T., and Zhong, S. J. Timescale and morphology of Martian mantle overturn immediately following magma ocean solidification. *J. Geophys. Res. Planets*, 119(3):454–467, 2014. doi: 10.1002/2013JE004496.
- Scheinberg, A., Soderlund, K. M., and Schubert, G. Magnetic field generation in the lunar core: The role of inner core growth. *Icarus*, 254:62–71, 2015. doi: 10.1016/j.icarus.2015.03.013.
- Scheinberg, A. L., Soderlund, K. M., and Elkins-Tanton, L. T. A basal magma ocean dynamo to explain the early lunar magnetic field. *Earth Planet. Sci. Lett.*, 492:144–151, 2018.
- Schmidt, R. M. and Housen, K. R. Some recent advances in the scaling of impact and explosion cratering. *Int. J. Impact Engin.*, 5(1):543 – 560, 1987. doi: 10.1016/0734-743X(87)90069-8.
- Schubert, G. and Sandwell, D. T. A global survey of possible subduction sites on Venus. *Icarus*, 117(1):173–196, 1995. doi: 10.1006/icar.1995.1150.
- Schubert, G. and Spohn, T. Thermal history of Mars and the sulfur content of its core. *J. Geophys. Res.*, 95:14095–14104, 1990. doi: 10.1029/JB095iB09p14095.
- Segatz, M., Spohn, T., Ross, M. N., and Schubert, G. Tidal dissipation, surface heat flow, and figure of viscoelastic models of Io. *Icarus*, 75:187–206, 1988. doi: 10.1016/0019-1035(88)90001-2.
- Seidelmann, P. K., Archinal, B. A., A’Hearn, M. F., et al. Report of the IAU/IAG Working Group on cartographic coordinates and rotational elements: 2006. *Celestial Mech. Dynam. Ast.*, 98(3): 155–180, 2007. doi: 10.1007/s10569-007-9072-y.
- Shea, E. K., Weiss, B. P., Cassata, W. S., et al. A Long-Lived Lunar Core Dynamo. *Science*, 335(6067):453, 2012. doi: 10.1126/science.1215359.
- Shoemaker, E. M. Interpretation of lunar craters. In Kopal, Z., editor, *Physics and Astronomy of the Moon*. Academic Press, New York and London, 1962.
- Shoemaker, E. M. Asteroid and Comet Bombardment of the Earth. *Ann. Rev. Earth Planet. Sci.*, 11: 461, 1983. doi: 10.1146/annurev.ea.11.050183.002333.
- Sleep, N. H. Martian plate tectonics. *J. Geophys. Research*, 99(E3):5639–5655, 1994.
- Snyder, G. A., Taylor, L. A., and Neal, C. R. A chemical model for generating the sources of mare basalts: Combined equilibrium and fractional crystallization of the lunar magmasphere. *Geochim. Cosmochim. Acta*, 56(10):3809–3823, 1992. doi: 10.1016/0016-7037(92)90172-F.
- Solomatov, S. Magma ocean and primordial mantle differentiation. In Schubert, G., editor, *Treatise on Geophysics*, pages 81–104. Elsevier, 2015.
- Solomatov, V. S. and Stevenson, D. J. Suspension in convective layers and style of differentiation of a terrestrial magma ocean. *J. Geophys. Res.*, 98(E3):5375–5390, 1993. doi: 10.1029/92JE02948.

- Solomatov, V. S., Olson, P., and Stevenson, D. J. Entrainment from a bed of particles by thermal convection. *Earth and Planetary Science Letters*, 120(3-4):387–393, 1993. doi: 10.1016/0012-821X(93)90252-5.
- Solomon, S. C. Formation, history and energetics of cores in the terrestrial planets. *Phys. Earth. Planet. Inter.*, 19(2):168–182, 1979. doi: 10.1016/0031-9201(79)90081-5.
- Solomon, S. C. and Chaiken, J. Thermal expansion and thermal stress in the moon and terrestrial planets: clues to early thermal history. *Lun. Planet. Sci. Conf. Proc.*, 3:3229–3243, 1976.
- Solomon, S. C. and Head, J. W. Lunar mascon basin: lava filling, tectonics, and evolution of the lithosphere. *Rev. Geophys. Space Phys.*, 18:107–141, 1980. doi: 10.1029/RG018i001p00107.
- Solomon, S. C., Comer, R. P., and Head, J. W. The evolution of impact basins: viscous relaxation of topographic relief. *J. Geophys. Res.*, 87:3975–3992, 1982. doi: 10.1029/JB087iB05p03975.
- Spudis, P. D., Martin, D. J. P., and Kramer, G. Geology and composition of the Orientale Basin impact melt sheet. *J. Geophys. Res. Planets*, 119:19–29, 2014. doi: 10.1002/2013JE004521.
- Stanley, S., Bloxham, J., Hutchison, W. E., and Zuber, M. T. Thin shell dynamo models consistent with Mercury’s weak observed magnetic field [rapid communication]. *Earth Planet. Sci. Lett.*, 234(1-2):27–38, 2005. doi: 10.1016/j.epsl.2005.02.040.
- Stegman, D. R., Jellinek, A. M., Zatman, S. A., Baumgardner, J. R., and Richards, M. A. An early lunar core dynamo driven by thermochemical mantle convection. *Nature*, 421(6919):143–146, 2003. doi: 10.1038/nature01267.
- Stevenson, D. J., Spohn, T., and Schubert, G. Magnetism and thermal evolution of the terrestrial planets. *Icarus*, 54:466–489, 1983. doi: 10.1016/0019-1035(83)90241-5.
- Stixrude, L., de Koker, N., Sun, N., Mookherjee, M., and Karki, B. B. Thermodynamics of silicate liquids in the deep Earth. *Earth Planet. Sci. Lett.*, 278(3-4):226–232, 2009. doi: 10.1016/j.epsl.2008.12.006.
- Stöffler, D. and Ryder, G. Stratigraphy and Isotope Ages of Lunar Geologic Units: Chronological Standard for the Inner Solar System. *Space Sci. Rev.*, 96:9–54, 2001.
- Strom, R. G., Trask, N. J., and Guest, J. E. Tectonism and volcanism on Mercury. *J. Geophys. Res.*, 80:2478–2507, 1975. doi: 10.1029/JB080i017p02478.
- Strom, R. G., Malhotra, R., Zhi-Yong, X., et al. The inner solar system cratering record and the evolution of impactor populations. *Res. Ast. Astrophys.*, 15(3):407, 2015.
- Suavet, C., Weiss, B. P., Cassata, W. S., et al. Persistence and origin of the lunar core dynamo. *Proc. Nat. Acad. Sci.*, 110(21):8453–8458, 2013. doi: 10.1073/pnas.1300341110.
- Suckale, J., Sethian, J. A., Yu, J.-d., and Elkins-Tanton, L. T. Crystals stirred up: 1. Direct numerical simulations of crystal settling in nondilute magmatic suspensions. *J. Geophys. Res. Planets*, 117(E8):E08004, 2012. doi: 10.1029/2012JE004066.
- Tackley, P. J., Schubert, G., Glatzmaier, G. A., et al. Three-Dimensional Simulations of Mantle Convection in Io. *Icarus*, 149(1):79–93, 2001. doi: 10.1006/icar.2000.6536.
- Takahashi, F. and Matsushima, M. Dipolar and non-dipolar dynamos in a thin shell geometry with implications for the magnetic field of Mercury. *Geophys. Res. Lett.*, 33(10):L10202, 2006. doi: 10.1029/2006GL025792.
- Takahashi, F., Shimizu, H., and Tsunakawa, H. Mercury’s anomalous magnetic field caused by a symmetry-breaking self-regulating dynamo. *Nature Comm.*, 10:208, 2019. doi: 10.1038/s41467-018-08213-7.

- Taylor, G. J. The bulk composition of Mars. *Chemie der Erde / Geochemistry*, 73(4):401–420, 2013. doi: 10.1016/j.chemer.2013.09.006.
- Taylor, G. J. and Wieczorek, M. A. Lunar bulk chemical composition: a post-gravity recovery and interior laboratory reassessment. *Phil. Trans. R. Soc. A*, 372(2024):20130242, 2014.
- Taylor, S. R. and McLennan, S. M. *Planetary Crusts: Their Composition, Origin and Evolution*. Cambridge Planetary Science. Cambridge University Press, Cambridge, UK, 2009. ISBN 9780521841863.
- Tian, Z., Zuber, M. T., and Stanley, S. Magnetic field modeling for Mercury using dynamo models with a stable layer and laterally variable heat flux. *Icarus*, 260:263–268, 2015. doi: 10.1016/j.icarus.2015.07.019.
- Tikoo, S. M., Weiss, B. P., Cassata, W. S., et al. Decline of the lunar core dynamo. *Earth Planet. Sci. Lett.*, 404:89–97, 2014. doi: 10.1016/j.epsl.2014.07.010.
- Tikoo, S. M., Weiss, B. P., Shuster, D. L., et al. A two-billion-year history for the lunar dynamo. *Sci. Adv.*, 3(8):e1700207, 2017. doi: 10.1126/sciadv.1700207.
- Tonks, W. B. and Melosh, H. J. The physics of crystal settling and suspension in a turbulent magma ocean. In Newsom, H. E. and Jones, J. H., editors, *Origin of the Earth*, pages 151–174. Oxford University Press, 1990.
- Tosi, N., Grott, M., Plesa, A.-C., and Breuer, D. Thermochemical evolution of Mercury’s interior. *J. Geophys. Res. Planets*, 118:2474–2487, 2013a. doi: 10.1002/jgre.20168.
- Tosi, N., Plesa, A. C., and Breuer, D. Overturn and evolution of a crystallized magma ocean: A numerical parameter study for Mars. *J. Geophys. Res. Planets*, 118(7):1512–1528, 2013b. doi: 10.1002/jgre.20109.
- Tosi, N., Čadež, O., Běhouňková, M., et al. Mercury’s low-degree geoid and topography controlled by insolation-driven elastic deformation. *Geophys. Res. Lett.*, 42:7327–7335, 2015. doi: 10.1002/2015GL065314.
- Tsunakawa, H., Takahashi, F., Shimizu, H., Shibuya, H., and Matsushima, M. Surface vector mapping of magnetic anomalies over the Moon using Kaguya and Lunar Prospector observations. *J. Geophys. Res. Planets*, 120(6):1160–1185, 2015. doi: 10.1002/2014JE004785.
- Turcotte, D. L. and Schubert, G. *Geodynamics*. Cambridge University Press, Cambridge, UK, 2<sup>nd</sup> edition, 2002. doi: 10.2277/0521661862.
- Vander Kaaden, K. E. and McCubbin, F. M. Exotic crust formation on Mercury: Consequences of a shallow, FeO-poor mantle. *J. Geophys. Res. Planets*, 120(2):195–209, 2015. doi: 10.1002/2014JE004733.
- Vaughan, W. M. and Head, J. W. Impact melt differentiation in the South Pole-Aitken basin: Some observations and speculations. *Planet. Space Sc.*, 91:101–106, 2014. doi: 10.1016/j.pss.2013.11.010.
- Šrámek, O. and Zhong, S. Martian crustal dichotomy and Tharsis formation by partial melting coupled to early plume migration. *J. Geophys. Res. Planets*, 117(E1):E01005, 2012. doi: 10.1029/2011JE003867.
- Warren, P. H. The magma ocean concept and lunar evolution. *Ann. Rev. Earth Planet. Sci.*, 13: 201–240, 1985. doi: 10.1146/annurev.ea.13.050185.001221.
- Warren, P. H. and Rasmussen, K. L. Megaregolith insulation, internal temperatures, and bulk uranium content of the moon. *J. Geophys. Res.*, 92:3453–3465, 1987. doi: 10.1029/JB092iB05p03453.
- Watters, T. R. and Johnson, C. L. Lunar tectonics. In Watters, T. R. and Schulz, R. A., editors, *Planetary tectonics*, pages 121 – 182. Cambridge Univ. Press, 2010.

- Watters, T. R., Robinson, M. S., Bina, C. R., and Spudis, P. D. Thrust faults and the global contraction of Mercury. *Geophys. Res. Lett.*, 31(4):L04701, 2004. doi: 10.1029/2003GL019171.
- Watters, T. R., Robinson, M. S., Beyer, R. A., et al. Evidence of recent thrust faulting on the moon revealed by the lunar reconnaissance orbiter camera. *Science*, 329(5994):936–940, 2010.
- Watters, W. A., Zuber, M. T., and Hager, B. H. Thermal perturbations caused by large impacts and consequences for mantle convection. *J. Geophys. Res. Planets*, 114:E02001, 2009. doi: 10.1029/2007JE002964.
- Weber, R. C., Lin, P.-Y., Garnero, E. J., Williams, Q., and Lognonné, P. Seismic detection of the lunar core. *Science*, 331:309–312, 2011. doi: 10.1126/science.1199375.
- Weiss, B. P. and Tikoo, S. M. The lunar dynamo. *Science*, 346(6214):1246753, 2014.
- Werner, S. C. The global martian volcanic evolutionary history. *Icarus*, 201(1):44–68, 2009.
- Whitaker, E. A. The lunar Procellarum basin. In Merrill, R. B. and Schultz, P. H., editors, *Multi-ring basins: Formation and Evolution*, pages 105–111, 1981.
- White, S. M., Crisp, J. A., and Spera, F. J. Long-term volumetric eruption rates and magma budgets. *Geochem. Geophys. Geosys.*, 7:Q03010, 2006. doi: 10.1029/2005GC001002.
- Whitten, J., Head, J. W., Staid, M., et al. Lunar mare deposits associated with the Orientale impact basin: New insights into mineralogy, history, mode of emplacement, and relation to Orientale Basin evolution from Moon Mineralogy Mapper (M<sup>3</sup>) data from Chandrayaan-1. *Journal of Geophysical Research (Planets)*, 116:E00G09, 2011. doi: 10.1029/2010JE003736.
- Wicht, J. and Heyner, D. Mercury’s magnetic field in the messenger era. In Shuanggen, J., editor, *Planetary Geodesy and Remote Sensing*. CRC Press, 2014.
- Wieczorek, M. A. Gravity and topography of the terrestrial planets. In Schubert, J., editor, *Planets and Moons* edited by T. Spohn, *Treatise on Geophysics, Vol. 10*. Elsevier, Amsterdam, The Netherlands, 2<sup>nd</sup> edition, 2015.
- Wieczorek, M. A. and Phillips, R. J. The structure and compensation of the lunar highland crust. *J. Geophys. Res.*, 102:10933–10944, 1997. doi: 10.1029/97JE00666.
- Wieczorek, M. A. and Zuber, M. T. Thickness of the Martian crust: Improved constraints from geoid-to-topography ratios. *J. Geophys. Res. Planets*, 109:E01009, 2004. doi: 10.1029/2003JE002153.
- Wieczorek, M. A., Jolliff, B. L., Khan, A., et al. The constitution and structure of the lunar interior. *Rev. Mineral. Geochem.*, 60:221–364, 2006. doi: 10.2138/rmg.2006.60.3.
- Wieczorek, M. A., Neumann, G. A., Nimmo, F., et al. The Crust of the Moon as Seen by GRAIL. *Science*, 339:671–675, 2013. doi: 10.1126/science.1231530.
- Wieczorek, M. A. Strength, depth, and geometry of magnetic sources in the crust of the moon from localized power spectrum analysis. *J. Geophys. Res. Planets*, 123(1):291–316, 2018.
- Williams, J.-P. and Nimmo, F. Thermal evolution of the Martian core: Implications for an early dynamo. *Geology*, 32(2):97, 2004. doi: 10.1130/G19975.1.
- Wood, J. A., Dickey Jr, J., Marvin, U. B., and Powell, B. Lunar anorthosites and a geophysical model of the moon. *Geochim. Cosmochim. Acta Supp.*, 1:965, 1970.
- Wünnemann, K., Collins, G. S., and Melosh, H. J. A strain-based porosity model for use in hydrocode simulations of impacts and implications for transient crater growth in porous targets. *Icarus*, 180: 514–527, 2006. doi: 10.1016/j.icarus.2005.10.013.

- Yu, S., Tosi, N., Schwinger, S., et al. Overturn of ilmenite-bearing cumulates in a rheologically weak lunar mantle. *J. Geophys. Res. Planets*, 124(2):418–436, 2019.
- Zhang, N., Parmentier, E. M., and Liang, Y. A 3-D numerical study of the thermal evolution of the Moon after cumulate mantle overturn: The importance of rheology and core solidification. *J. Geophys. Res. Planets*, 118:1789–1804, 2013a. doi: 10.1002/jgre.20121.
- Zhang, N., Parmentier, E. M., and Liang, Y. Effects of lunar cumulate mantle overturn and megaregolith on the expansion and contraction history of the Moon. *Geophys. Res. Lett.*, 40(19):5019–5023, 2013b. doi: 10.1002/grl.50988.
- Zhang, N., Dygert, N., Liang, Y., and Parmentier, E. M. The effect of ilmenite viscosity on the dynamics and evolution of an overturned lunar cumulate mantle. *Geophys. Res. Lett.*, 44(13): 6543–6552, 2017. doi: 10.1002/2017GL073702.
- Zhao, Y., de Vries, J., van den Berg, A. P., Jacobs, M. H. G., and van Westrenen, W. The participation of ilmenite-bearing cumulates in lunar mantle overturn. *Earth Planet. Sci. Lett.*, 511:1–11, 2019. doi: 10.1016/j.epsl.2019.01.022.
- Zhong, S., Parmentier, E. M., and Zuber, M. T. A dynamic origin for the global asymmetry of lunar mare basalts. *Earth Planet. Sci. Lett.*, 177(3-4):131–140, 2000. doi: 10.1016/S0012-821X(00)00041-8.
- Zhu, M.-H., Wünnemann, K., Potter, R. W., Kleine, T., and Morbidelli, A. Are the Moon’s Nearside-Farside Asymmetries the Result of a Giant Impact? *J. Geophys. Res. Planets*, 124(0):1–24, 2019. doi: 10.1029/2018JE005826.
- Ziegler, L. B. and Stegman, D. R. Implications of a long-lived basal magma ocean in generating Earth’s ancient magnetic field. *Geochem. Geophys. Geosyst.*, 14(11):4735–4742, 2013. doi: 10.1002/2013GC005001.
- Zolotov, M. Y., Sprague, A. L., Hauck, S. A., II, et al. The redox state, FeO content, and origin of sulfur-rich magmas on Mercury. *J. Geophys. Res. Planets*, 118:138–146, 2013. doi: 10.1029/2012JE004274.